

Key Points:

- The 2012 M_w 7.5 Ometepec–Pinotepa Nacional earthquake caused a long-term increase in the surrounding slip rates that lasted at least 6 years
- Unlocking of a near the trench block favored the rupture of the 2018 M_w 7.2 Pinotepa Nacional earthquake
- Coda wave interferometry analysis asserts that repeating earthquakes are caused by the same asperity

Supporting Information:

Supporting Information may be found in the online version of this article.

Correspondence to:

L. A. Dominguez,
ladominguez@igeofisica.unam.mx

Citation:









Dominguez, L. A., Taira, T., Cruz-Atienza, V. M., Iglesias, A., Villafuerte, C., Legrand, D., et al. (2022). Interplate slip rate variation between closely spaced earthquakes in southern Mexico: The 2012 Ometepec and 2018 Pinotepa Nacional thrust events. *Journal of Geophysical Research: Solid Earth*, 127, e2022JB024292. <https://doi.org/10.1029/2022JB024292>

Received 26 FEB 2022
Accepted 2 JUN 2022

Author Contributions:

Conceptualization: L. A. Dominguez, T. Taira, V. M. Cruz-Atienza, A. Iglesias
Formal analysis: L. A. Dominguez
Funding acquisition: L. A. Dominguez, T. Taira, V. M. Cruz-Atienza
Investigation: L. A. Dominguez, T. Taira, V. M. Cruz-Atienza, C. Villafuerte, X. Pérez-Campos
Methodology: T. Taira, V. M. Cruz-Atienza, X. Pérez-Campos
Resources: D. Legrand, M. Raggi
Software: L. A. Dominguez, T. Taira, V. M. Cruz-Atienza, A. Iglesias, X. Pérez-Campos, M. Raggi
Validation: L. A. Dominguez, T. Taira, V. M. Cruz-Atienza, X. Pérez-Campos

Interplate Slip Rate Variation Between Closely Spaced Earthquakes in Southern Mexico: The 2012 Ometepec and 2018 Pinotepa Nacional Thrust Events

L. A. Dominguez^{1,2} , T. Taira³ , V. M. Cruz-Atienza² , A. Iglesias² , C. Villafuerte^{2,4} , D. Legrand² , X. Pérez-Campos² , and M. Raggi¹ 

¹Escuela Nacional de Estudios Superiores, Unidad Morelia, Universidad Nacional Autónoma de México, Morelia, México, ²Instituto de Geofísica, Universidad Nacional Autónoma de México, Mexico City, Mexico, ³Berkeley Seismological Laboratory, University of California, Berkeley, CA, USA, ⁴Now at Laboratoire de Géologie, Département de Géosciences, École Normale Supérieure, CNRS, UMR 8538, PSL Université, Paris, France

Abstract On 20 March 2012, a M_w 7.5 thrust earthquake started a series of seven large events ($7.0 \leq M_w \leq 8.2$) that struck central Mexico during a period of 9 years (2012–2021). Before this event, the Mexican subduction zone did not experience significant subduction earthquakes ($M_w > 7.0$) for at least 12 years. Five of the events occurred in the plate interface, resulting in a significantly larger interplate slip rate in the states of Oaxaca and Guerrero. In this study, we explore how an aseismic slip transient caused by the 2012 M_w 7.5 earthquake affected the Oaxaca region and whether this earthquake had a causal relationship with the M_w 7.2 Pinotepa Nacional event that took place six years later in a nearby zone. To this end, we identified and analyzed characteristic repeating earthquakes along the Mexican subduction zone for assessing the plate interface slip history and found a remarkable increase in the aseismic slip rate following the 2012 mainshock, which suggests a long-standing slip perturbation near the trench in Oaxaca that continued until the Pinotepa Nacional earthquake of 2018.

Plain Language Summary This study analyzes the large increase in seismicity and the changes in the plate interface motion that occurred between two major thrust earthquakes: the 2012 M_w 7.5 Ometepec earthquake and the 2018 M_w 7.2 Pinotepa Nacional earthquake. These two events, located in the state of Oaxaca in southern Mexico, were produced by two nearby asperities whose hypocenters were separated by only ~60 km. To estimate the interseismic slip rates, we analyzed the occurrence of repeating events, a type of earthquake believed to be the result of asperities on the plate interface that rupture the same patch at relatively regular intervals. This kind of earthquake has extraordinarily similar waveforms that suggest a common origin in space and a similar rupture process. We explored the repeating earthquake activity and its characteristics to determine how the induced seismicity produced by the 2012 Ometepec earthquake influenced the rupture of the 2018 Pinotepa Nacional earthquake.

1. Introduction

An intense increase in seismic activity that may last from a few weeks or months through several decades often follows long quiescent seismic periods (Stein & Liu, 2009). While many earthquakes are clustered in both space and time (Barbot et al., 2012; Konca et al., 2008; Santoyo et al., 2005), others occur spontaneously with no clear triggering mechanisms (Corral, 2004; Kagan & Jackson, 1991; Kanamori, 1981; Keilis-Borok et al., 1980; Q. Wang et al., 2010; Wyss & Habermann, 1988). In this regard, the Ometepec–Pinotepa Nacional region is a remarkable example of an area that experiences modulated periods of seismic activity. This segment, located along the central Pacific coast of Mexico at the border between the Oaxaca and Guerrero states, is well known for the occurrence of large earthquakes ($\geq M7.0$) that often take place as pairs of events interacting with each other during a relatively short period (Yamamoto et al., 2002). The most striking example happened in 1982, when a magnitude M_s 7.0 earthquake was preceded by a M_s 6.9 earthquake within 5 hr (Astiz & Kanamori, 1984). Another duplet-type event occurred in 1928 when a magnitude M_s 7.6 was preceded by a M_s 7.4 two months before (Singh et al., 1981). A similar scenario occurred in 1962 to the West of the Ometepec–Pinotepa Nacional region, when a magnitude M_s 7.2 was followed by a M_s 6.9 only 8 days apart (Nishenko & Singh, 1987; Ortiz et al., 2000). Furthermore, in 1995 and 1996, two earthquakes with magnitudes larger than 7.0 ruptured within a

Writing – original draft: L. A. Dominguez, T. Taira, V. M. Cruz-Atienza, C. Villafuerte, D. Legrand, X. Pérez-Campos, M. Raggi
Writing – review & editing: L. A. Dominguez, T. Taira, V. M. Cruz-Atienza, A. Iglesias, C. Villafuerte, D. Legrand, X. Pérez-Campos

year (Anderson et al., 1995; Singh et al., 1997). Other magnitude M 7.0 events occurred as single earthquakes in 1937 (M_s 7.7), 1948 (M_s 7.0), 1950 (M_s 7.3), and 1968 (M_s 7.3; see inset Figure 1). Recently, this area experienced two more earthquakes that ruptured a few years apart, the first one happened on 20 March 2012 (M_w 7.5; Universidad Nacional Autónoma de México [UNAM] Seismology Group, 2013) about 30 years after the 1982 doublet, and the second earthquake ruptured a nearby area, ~60 km apart, on 16 February 2018 (M_w 7.2; Li et al., 2020; Figure 1). The aftershock sequence of the 2012 earthquake was particularly productive compared to other Mexican earthquakes located along the trench. This earthquake is characterized by a high Gutenberg–Richter b value (1.50 ± 0.10) and a low Omori p -value (0.37 ± 0.12). Furthermore, the modulation of the aftershocks rate by the Earth tides strongly suggests the presence of highly pressurized fluids at the plate interface in this Oaxaca region (Legrand et al., 2021). Double type events had been observed worldwide on different tectonic environments (Kagan & Jackson, 1999). The short recurrence interval of this type of earthquakes conflicts with the long-term tectonic loading expected from the plate motion and poses a severe uncertainty for the short-term seismic hazard analysis (Kagan, 2011). Two main mechanisms for doublet rupture (or even multiple) have been proposed. One of them suggests that stress transfer along the same fault plane produces earthquakes with similar focal mechanism and magnitudes (e.g., Astiz & Kanamori, 1984; Cleveland et al., 2014; Lay et al., 2010). The second mechanism involves a complex interaction between nearby adjacent faults (Cesca et al., 2021; Horikawa, 2001; Lay et al., 2009; Yin-Tung et al., 2008). In this study, we evaluate the space–time evolution of the slip rate in this region between these two events, the 2012 and 2018 earthquakes and compare it with adjacent segments to understand the high seismicity rate in this area that has persisted for nearly a century of instrumental seismology.

Recent advances in seismic and geodetic monitoring have provided new evidence about the possible mechanisms that cause such a high interplate slip rate compared to adjacent areas. Geodetic instrumentation shows that this area is constantly influenced by the occurrence of slow slip events (SSEs) downdip the Ometepec–Pinotepa Nacional segment every 1–2 years ($\sim M6.0$) which may have a strong influence on the occurrence of megathrust earthquakes in the region (Figure 1; Cruz-Atienza et al., 2021; Graham et al., 2014). To the West, in the state of Guerrero, there is a region where no earthquakes with a magnitude larger than $M > 7.0$ have occurred in more than a hundred years known as the Guerrero Gap (GG; Singh et al., 1981; Universidad Nacional Autónoma de México [UNAM] Seismology Group, 2015), where downdip SSEs take place every ~4 years (Radiguet et al., 2012; Vergnolle et al., 2010). In addition, tectonic tremor has been observed most energetically in Oaxaca and Guerrero (Cruz-Atienza et al., 2015, 2018; A. Husker et al., 2019; A. L. Husker et al., 2012; Kostoglodov et al., 2010; Payero et al., 2008; Rivet et al., 2014; Villafuerte & Cruz-Atienza, 2017), and near the trench (Plata-Martínez et al., 2021). Tremors form an almost continuous belt that extends from the state of Colima in the West through Oaxaca in the East, where very low frequency earthquakes appear during tremor activity (Maury et al., 2016, 2018). This variety of mechanisms has led to several hypotheses about the seismic budget distribution (Gualandi et al., 2017; Radiguet et al., 2012; Ramírez-Herrera et al., 2018) that suggest that a significant portion of the stress is released through aseismic slip in the seismic gap including its offshore segment (Plata-Martínez et al., 2021). If these hypotheses held true, the GG would not likely have yet the potential to nucleate large megathrust earthquakes by itself. Nonetheless, larger ruptures may be able to transit from either side as Plata-Martínez et al. (2021) hypothesized, which could lead to $M > 8.0$ earthquake in Guerrero.

1.1. Tectonic Overview

The Mexican subduction zone is the result of the fragmentation of the Farallon plate that caused the oblique subduction of the oceanic Cocos and Rivera plates (Lonsdale, 2005) beneath the continental North America plate. The resulting configuration produced a wide flat subducting slab that extends from the coast up to 250 km inland, flanked by segments with a steeper slope on both sides (Kim et al., 2013; Pardo & Suárez, 1995; Stubailo et al., 2012). The geometry of the slab has been explored using a wide range of techniques such as earthquake relocation (Pardo & Suárez, 1995), receiver functions (Melgar & Pérez-Campos, 2011; Pérez-Campos et al., 2008), seismic ambient noise (Castellanos et al., 2018; Gaite et al., 2012; Spica et al., 2016), surface waves (Iglesias et al., 2010; Stubailo et al., 2012), body wave tomography (A. Husker & Davis, 2009), and seismic attenuation (T. Chen & Clayton, 2012). Flattening of the slab is likely due to dehydration and rollback that caused a shift in the volcanic arc which lies oblique with an angle of $\sim 15^\circ$ with respect to the trench, forming the Trans-Mexican volcanic belt with very diverse chemical signatures (Ferrari et al., 2012, and references therein; Skinner & Clayton, 2011). Another relevant feature for the regional tectonics consists of a continental left-lateral 650 km long fault system that extends parallel to the trench that accommodates a significant part of the oblique

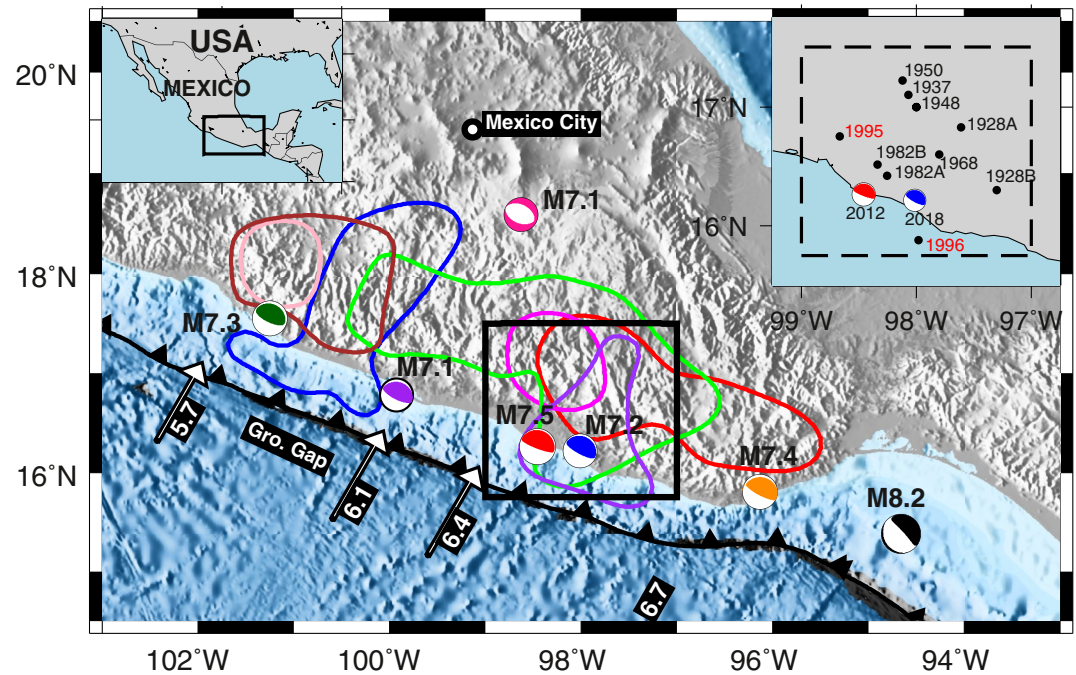


Figure 1. Major earthquakes in 2012–2020 in Mexico and significant seismicity ($M \geq 6.9$) in the Ometepec–Pinotepa National region. Beach balls indicate the focal mechanisms of $M_w > 7$ earthquakes during the 2001–2021 period (red, 2012 Ometepec earthquake; green, 2014 Papanoa earthquake; blue, 2018 Pinotepa Nacional earthquake; black, 2017 Tehuantepec earthquake; pink, 2017 Puebla–Morelos earthquake; orange, 2020 La Crucecita earthquake; purple, 2021 Acapulco earthquake). Colored contours show the rupture areas of the reported slow slip events (SSEs) and the aftership of the 2018 Pinotepa earthquake determined by Cruz-Atienza et al. (2021) (blue, Guerrero SSE 2017; red, Oaxaca SSE 2017–2018; green, Guerrero–Oaxaca SSE 2018; pink, Oaxaca SSE 2018; purple, Oaxaca SSE 2018; brown, Guerrero SSE 2019). Inset indicates known estimated hypocenters of large events ($M \geq 6.9$) since 1901 (Sawires et al., 2019). The black dashed rectangle indicates the region of interest.

component of the subducting slab (Kazachkina et al., 2019, 2020). Both earthquake swarms and SSEs have been detected at the interface of this fault system in Oaxaca (Fasola et al., 2019).

1.2. Pore Pressure and Fluids in the Ometepec–Pinotepa National Region

Considerable evidence suggests that the release of fluids controls the seismicity in this region. To the West, using magnetotelluric measurements in Guerrero, A. Husker et al. (2018) found a high conductivity zone on the upper layer of the subducting slab, which was associated with the presence of highly pressurized fluids as observed in different regions of the globe (Audet & Kim, 2016) and that may explain the migration pattern of tectonic tremor and SSE cycles in that state and globally (Cruz-Atienza et al., 2018; Warren-Smith et al., 2019). In the Ometepec–Pinotepa segment, Plata-Martínez et al. (2019) examined the radiated energy of aftershock sequences of both the 2012 M_w 7.5 Ometepec–Pinotepa Nacional (hereafter 2012 Ometepec earthquake) and the 2018 M_w 7.2 Pinotepa Nacional earthquakes (hereafter 2018 Pinotepa earthquake). The ratio between the seismic energy to the seismic moment also suggests the presence of fluids along this zone. Elevated pore pressure can significantly reduce the effective normal stress allowing a higher seismicity rate compared to areas with lower fluid content. This was made clear by Legrand et al. (2021), who identified tidal-modulated aftershock seismicity following the 2012 M_w 7.5 Ometepec earthquake, and a high Gutenberg–Richter b value and low Omori p -value, suggesting again the presence of overpressurized fluids largely affecting the aftershock productivity. Fluids are often considered a major player that regulates the seismic activity that may result in large megathrust earthquakes (Audet & Schwartz, 2013; Moreno et al., 2014) and quantitatively explain the cycle of slow earthquakes at the plate interface (Warren-Smith et al., 2019), including their associated rapid migrations (Cruz-Atienza et al., 2018).

2. Data

We extended the repeating earthquakes (REs, or repeaters) analysis, presented in Dominguez et al. (2016), by incorporating a longer time window ranging from 2001 through October 2021 (former results spanned from 2001 through 2014). Additionally, we carried out a complementary analysis of the rupture characteristics of the individual earthquakes to identify RE pairs. In total, we examined 440,655 vertical-component waveforms from 75,567 earthquakes ($M_c > 1.5$) reported by the Servicio Sismológico Nacional (Pérez-Campos et al., 2018; Servicio Sismológico Nacional [SSN], 2021). Coda magnitude (M_c) is estimated as shown in Pérez-Campos et al. (2019). Figure S1 in Supporting Information S1 shows the data availability and the number of records per event, as well as their magnitude distribution. Large gaps exist in the waveform data before 2006; therefore, caution must be taken in the interpretation of the results between 2001 and 2006. As of October 2021, all the stations have a sample rate of at least 100 Hz. Nonetheless, historical waveforms at some stations (i.e., CAIG, before 2008; MEIG, before 2014; OXIG, before 2007; PLIG, before 2008; and PNIG, before 2007) are only available at 20 Hz, though. Therefore, we downsampled all records to 20 samples per second for our RE detections for this study. Notice that stations YOIG and PEIG were installed after the 2012 Ometepe earthquake. Thus, these stations will not be considered to evaluate temporal changes in RE activity before and after this earthquake.

3. Methods

3.1. Repeating Earthquakes

REs are a type of event that consistently ruptures the same patch along the fault plane producing remarkably similar waveforms when examined at the same stations at different times (Poupinet et al., 1984; Vidale et al., 1994). Unlike most of the earthquakes which show complex and Poisson-type behavior, REs have relatively predictable recurrence times that scale with moment magnitude as $\sim M^{1/6}$ (Cattania & Segall, 2019; T. Chen & Lapusta, 2009; Nadeau & Johnson, 1998). REs are therefore considered the result of asperities that systematically accumulate and release stress with a similar moment magnitude in an otherwise aseismic slipping area. This process has been reported in a wide variety of tectonic environments such as oceanic fracture zones (Materna et al., 2018), transform faults (Nadeau & McEvilly, 1999, 2004; Uchida et al., 2019; Vidale et al., 1994), volcanoes (Tepp, 2018), and subduction zones (Chaves et al., 2020; Hughes et al., 2021; Mavrommatis et al., 2015; Uchida et al., 2015). Monitoring REs thus allows the estimation of the interplate aseismic slip as well as examining changes in the mechanical properties of the fault system. Nadeau and Johnson (1998) proposed an empirical relationship that links the interface slip around the seismogenic asperity, d , as a function of the RE coseismic moment, M_0 , given by

$$d = 10^a M_0^b \quad (1)$$

where a and b are empirical constants. These authors suggested the following values $a = -2.36$ and $b = 0.17$ based on REs from Parkfield, California. Subsequent reevaluations of these constants for the San Andreas fault suggested updated values of $a = -1.09 \pm 0.2$ and $b = 0.10 \pm 0.02$ (Nadeau & McEvilly, 2004); and $a = -1.53 \pm 0.37$ and $b = 0.10 \pm 0.02$ (Khoshmanesh et al., 2015).

We identified REs by comparing waveforms from pairs of nearby events (i.e., epicentral distances smaller than 50 km) reported in the SSN local catalog (SSN, 2021) with a 25 s time window from the onset of the P wave, which includes both P and S wave arrivals for events within 300 km from the station. Data were demeaned, detrended and filtered using a Butterworth band-pass filter between 2 and 8 Hz. Then, we estimated the correlation coefficient and spectral coherency. We declared a pair of events as REs when both the correlation coefficient and the spectral coherence exceeded 0.95 for at least two stations. Sequences were initially formed by combining those pairs of events that shared a common reference earthquake into a single group. For example, suppose earthquakes A and C have a correlation coefficient and spectral coherency equal or higher than the given threshold (95%). In that case, we declare them as members of a RE sequence. Furthermore, suppose the waveform from a third event, earthquake B, meets the same similarity criterium compared to either earthquake A or C (not necessarily both). In that case, earthquake B is also a member so that all three events (A–C) constitute a single sequence of REs. In the following sections, we detail our strategy to minimize false RE detections, which includes an additional constrain (unlike the study by Dominguez et al., 2016) where we estimated the relative distances between pairs of events using coda interferometry (Snieder & Vrijlandt, 2005) and inverted the results to make sure that

the same asperity is indeed at the origin of the events instead of nearby asperities with a very similar earthquake to station path. The asperity size of each earthquake was determined independently through a stress drop estimate.

3.2. Stress Drops Calculation

To determine the size of the rupture patches and thus whether a sequence of repeaters was produced by the same asperity or by a nearby asperity, we first computed the stress drop of each seismic event based on Brune's model (Brune, 1970). Our procedure is similar to that proposed by Ordaz and Singh (1992), although we solved for the stress drop assuming the attenuation laws presented in García et al. (2009). The observed spectrum at the station i for the j event may be expressed as

$$A_{ij}(f, R_{ij}) = C \cdot S_j(f) \cdot G(R_{ij}) \cdot e^{-\frac{\pi f \cdot R_{ij}}{Q(f)}}, \quad (2)$$

where f is the frequency, R_{ij} is the hypocentral distance, $G(R_{ij})$ is the geometrical spreading, $Q(f)$ is the attenuation, and

$$C = \frac{R_{\theta\phi} F}{4\pi \rho v^3} \quad (3)$$

In this equation, $R_{\theta\phi} = 0.55$ represents the average radiation pattern (Boore & Boatwright, 1984), $F = 2.0$ accounts for the free surface amplification, v is the P wave velocity (6,230 m/s), and the density $\rho = 2.7 \text{ g/cm}^3$ (García et al., 2004). We used a path-dependent attenuation function and distance-dependent geometrical spreading as shown in García et al. (2009) for the Mexican subduction zone where $Q_S(f) = 175 f^{0.52}$ for coastal paths and $Q_S(f) = 211 f^{0.46}$ otherwise. To estimate the equivalent $Q_P(f)$ attenuation, we considered that $Q_P^{-1} = (4/9)Q_S^{-1}$ for a Poisson solid (Shearer, 2019), assuming the same frequency dependence. Thus, we obtained $Q_P(f) = 394 f^{0.52}$ for coastal paths and $Q_P(f) = 475 f^{0.46}$ otherwise. The geometrical spreading is defined as

$$G(R) = \begin{cases} 1/r, & \text{for } r < 50 \text{ km} \\ 1/\sqrt{50r}, & \text{for } r \geq 50 \text{ km} \end{cases} \quad (4)$$

for coastal paths, and

$$G(R) = \begin{cases} 1/r, & \text{for } r < 50 \text{ km.} \\ 1/50, & \text{for } 50 \leq r \leq 150 \text{ km} \\ \sqrt{3}/\sqrt{50r}, & \text{for } r \geq 150 \text{ km} \end{cases} \quad (5)$$

for trajectories toward the continent. For the instrument response, we applied a prefilter with the following corner frequencies $f_c = 0.005, 0.0125, 30, 40$ Hz. After correcting path effects, we took a P wave time window of 1.28 s (128 samples at 100 sampling rate) and applied a 5% taper to the signal. Brune's model allows estimating the source dimensions from the power spectra of either the P wave or the S wave at the source, which can be approximated as

$$S(f) = \frac{\Omega_0 (2\pi f)^m}{1 + (f/f_c)^2}, \quad (6)$$

where $S(f)$ is the spectrum of the seismic recording after removing the geometrical spreading, attenuation, and the instrument response. m is a factor that is applied in the frequency domain depending on whether the spectrum is on displacement ($m = 0$), velocity ($m = 1$), or acceleration ($m = 2$), f_c is the corner frequency and Ω_0 is the flat level at low frequencies in the displacement spectrum. We used a multitaper spectrum library to estimate the spectrum as shown by Prieto (2022) and fit the resulting spectrum for all three possible combinations of spectra (displacement, velocity, and acceleration) for the vertical component. Then, we estimated the coefficient

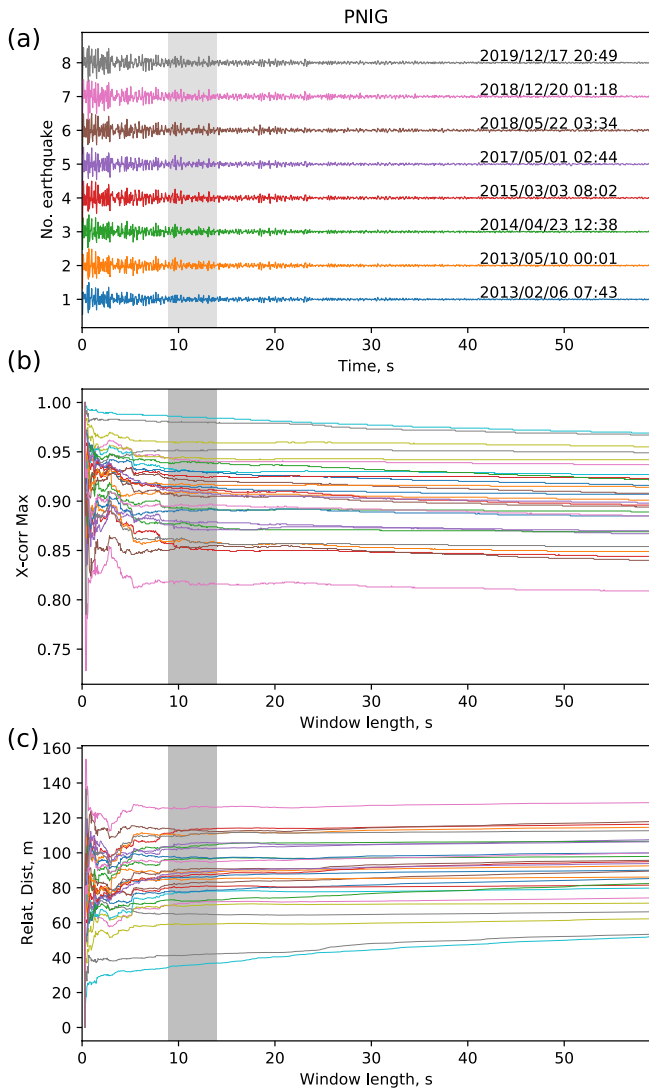


Figure 2. Coda wave interferometry results for sequence 0406. This repeating earthquake (RE) sequence consists of eight members with a mean coda magnitude of $M_c = 3.9$. (a) Individual waveforms, the gray shaded area indicates the time window where the relative distance between events is calculated. (b) Maximum cross correlation and (c) relative distance between each pair of events. Time $t = 0$, corresponds to twice $S-P$ time measured from the onset of the P wave.

of determination, R^2 , and thus evaluated the goodness of the fitting. R^2 was computed as

$$R^2 = \left(1 - \frac{U_{residual}}{U_{total}}\right) \times 100, \quad (7)$$

where $U_{residual} = \sum (u_{obs} - u_{Brune})^2$ is the sum square of the residuals. $U_{total} = \sum (u_{obs} - \bar{u})^2$ is the total sum of squares, and \bar{u} indicates the mean value of the observed data. Finally, we estimate the stress drop, $\Delta\sigma$, as a function of the estimated seismic moment M_0 and the corner frequency f_c ,

$$\Delta\sigma = \frac{7}{16} \left(\frac{f_c}{\kappa\beta}\right)^3 M_0. \quad (8)$$

In this case, $\kappa = 0.32$ (Madariaga, 1976) and β is the S wave velocity (3.9 km/s) in the crust (Dziewonski & Anderson, 1981). To evaluate the stress drop for each cluster, we took the average values of the best fitting spectra with signal-to-noise ratio, $SNR \geq 5$, and $R^2 \geq 80\%$. Examples of the fittings are shown in Figure S2 in Supporting Information S1, and a summary of the results is provided in the Supporting Information Data Set S1.

3.3. Interevent Distance and Relative Positions

When two closely spaced asperities produce REs, the recorded waveforms exhibit a large correlation and coherence value. In this case, they can be produced either by a partial rupture of a larger asperity or by nearby independent asperities located a few meters apart (Uchida, 2019). We assumed that each rupture could be modeled as an instantaneous penny-shape circular crack whose radius is estimated from their moment magnitude and stress drop (Eshelby, 1957),

$$R = \left(\frac{7}{16} \frac{M_0}{\Delta\sigma}\right)^{1/3} \quad (9)$$

where M_0 is the moment magnitude in N m, and $\Delta\sigma$ is the stress drop in MPa. The relative distance between pairs of events was computed employing coda wave interferometry (Snieder & Vrijlandt, 2005). Figure 2 illustrates an example of this process. Figure 2a shows the waveforms of sequence 0406 that containing eight REs. First, we aligned all the waveforms to the P wave using a cross correlation of the entire waveform in a 51 s window. Analysis of the correlation coefficient starts in the coda, which we assumed starts at twice the $S-P$ arrival time. Then, we vary the window length and measure the distance in a 5 s window at three times the $S-P$ arrival time from the onset of the P wave. Figure 2b shows the variations of the correlation coefficient

as a function of the window length, and Figure 2c shows the corresponding interevent distance, as described by Snieder and Vrijlandt (2005), for all possible pairs.

Once we obtained a set of interevent distances for each RE sequence, we determined a plausible configuration of the hypocenter at the plane interface. To invert the relative interevent positions estimated by means of coda wave interferometry, we used a differential evolution algorithm approach (Storn & Price, 1997). This optimization method maintains a population of individuals (i.e., candidate solutions) that gradually minimize an objective function. In our cause, individuals are the hypocentral locations of each event along the same fault plane so that for every set of points is lying in the plane; the method finds the pairwise distance matrix D_P , where $D_P[i, j] = d(P_i, P_j)$. Among all such pairs, P , the optimal event locations are those minimizing the objective function $d(D, D_P)$. In this sense, differential evolution can be thought of as a primitive genetic algorithm. This

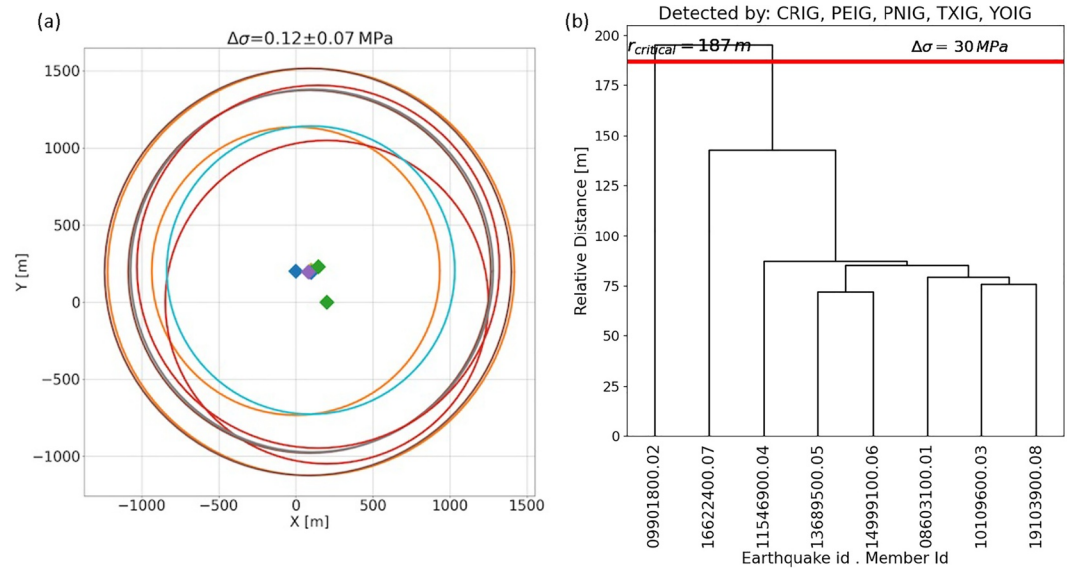


Figure 3. Relative locations and dendrogram of the sequence 0203. (a) Estimated relative locations and estimated rupture area for all events within the sequence. (b) Dendrogram, the x axis indicates the earthquake id and the consecutive member id within the sequence, the y axis indicates the relative distance.

method, in a nutshell, maintains a population of individuals that gradually improve. Therefore, each generation is constructed from the previous generation. To perform differential evolution, we start with a population of random individuals. Then, we successively repeat the following procedure: in each generation, for each individual P in the current population, we choose three other individuals A , B , and C ; and use them to construct a new candidate individual, which we will call, \tilde{P} . This candidate \tilde{P} is compared against P and replaced it in the next generation if its associated cost function is lower. This process continues until no more improvements are to be found; see Storn & Price (1997) for further details.

Figure 3 illustrates the process described above to examine sequence 0203. The estimated average stress drop for this sequence inferred from Brune's model fitting is $\Delta\sigma = 0.12 \pm 0.07$ MPa. The radius of the asperity is then computed using Equation 9. In this case, we assigned the same radius to all members based on their estimated stress drop and M_0 . Figure 3a shows a possible plane solution of relative locations and size of the asperity based on the inversion of their relative distances estimated using coda wave interferometry as explained previously. Notice that any rotation of the reference system will also be a solution to that specific set of relative distances. Figure 3b shows the dendrogram which indicates whether the members within the same sequences can be associated with a single asperity or not. In this specific example, the diagram suggests that a stress drop of at least $\Delta\sigma = 30$ MPa is required to obtain a separation distance short enough ($r_{critical} = 187$ m) to consider the earthquake 09901800.02 as an independent asperity. Therefore, in this case, we conclude that all earthquakes within the sequence belong to the same asperity given the estimated stress drop and their relative interevent distances.

3.4. Completeness of the RE Catalog

Since our RE detections detach from waveform templates of earthquakes reported by the SSN, our catalog's spatial completeness (i.e., the geographic extent with the same cutoff magnitude) of our catalog is tied to the detectability of the SSN instrumental network. Once stations YOIG and PEIG were installed in 2012, a completeness analysis of the station network (Figure S3 in Supporting Information S1) indicates that the current cutoff magnitude (M_c) is about 3.3 for the whole extent of our study area. However, to avoid apparent changes in the seismicity rate due to detectability artifacts in our long-term RE time series ranging between 2002 and 2020, we determined a sufficient minimum completeness value $M_c = 3.8$ which implies that most of the events above this magnitude have similar locations and focal mechanisms to the template earthquakes in our catalog within the geographic extent. In the following section, we will not consider any detection below this threshold to assure that

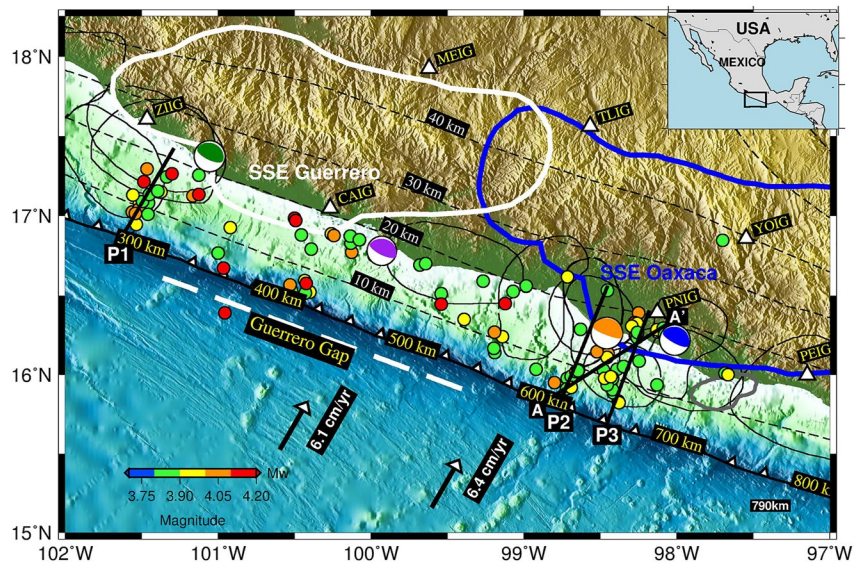


Figure 4. Detected repeating earthquake (RE) sequences along the Guerrero and Oaxaca megathrust above $M_c \geq 3.8$. Triangles indicate the location of the permanent seismic stations used in this study. The white dashed line shows the extension of the Guerrero Gap. Thick black lines indicate the location of the four profiles examined in this study. Focal mechanisms correspond to the recent $M_w > 7.0$ earthquakes: 2014 Papanoa earthquake (green), 2012 Ometepec earthquake (orange), 2018 Pinotepa earthquake (blue), and 2021 Acapulco earthquake (purple). RE clusters are indicated by circles color coded by mean magnitude. Black dashed lines show the slab isodepth as shown by Cruz-Atienza et al. (2021). Black closed contours represent rupture areas of large earthquakes (Kostoglodov & Pacheco, 1999). Thick contours approximate areas of slow slip event (SSE) ruptures areas in Guerrero (white) and Oaxaca (blue; Graham et al., 2014).

our interpretations are not influenced by improvements in the network. Nonetheless, complementary figures containing all detections are provided in the Supporting Information.

4. Results and Discussion

We found a set of 476 RE sequences that contain between 2 and 25 members with magnitudes ranging from 3.0 to 4.5 (see Supporting Information Data Set S2). The locations of the sequences are color coded according to their magnitude in Figure 4. As discussed above, on this map, we only include events that meet a strict completeness criterion of the earthquake catalog across the study region during the whole analyzed period (for a map including all detected RE see Figure S4 in Supporting Information S1). Notice that the GG and Puerto Escondido (i.e., close to PEIG station) segment stands out as areas with a lower concentration of REs compared to adjacent areas likely perturbed by the large subduction earthquakes. In comparison, the area of interest (Ometepec–Pinotepa Nacional region) exhibits a noticeable larger RE activity, as well as the offshore region of the 2014 Papanoa earthquake.

In Figure 5, we compare the changes in RE activity across both the Ometepec–Pinotepa Nacional and GG regions. Notice the drastic change in seismicity and, consequently, the number of REs following the 2012 Ometepec earthquake in the former case. In Figure 5a, we show the timing of significant nearby earthquakes ($M_w \geq 6.0$; blue and red dots for Oaxaca and Guerrero, respectively), the approximate duration of SSEs in Guerrero (red shaded areas) and Oaxaca (blue shaded areas), and the number of REs reported as a function of time in 2-month bins. We included in this plot the 2017 M_w 7.1 Puebla earthquake (Melgar, Ruiz-Angulo, et al., 2018; Singh et al., 2018), given their magnitude and societal impact. However, this event ruptured ~ 250 km from the trench in the bending section of the slab and no static or dynamic transfer of stress has been found (Cruz-Atienza et al., 2021; Segou & Parsons, 2018). Cumulative RE counts show that the Ometepec–Pinotepa Nacional segment almost doubled the activity observed in the GG during the study period (2012–2021; Figure 5b).

To compare the RE recurrence time interval with studies worldwide, we evaluated the recurrence times for the RE catalog as a function of the seismic moment, M_0 . Figure 6 shows the results color coded by their position along the trench, as indicated in the inset. REs along the GG (red-orange colors diamond markers) have recurrence times ranging between 1 and 10 years, which are generally consistent with the Nadeau and Johnson (1998)

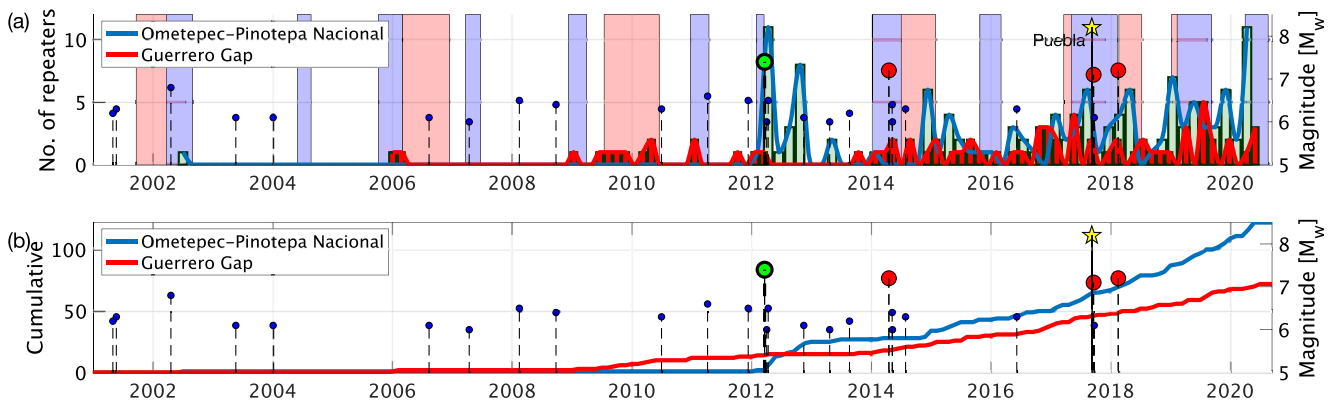


Figure 5. Major earthquakes and cumulative number of repeating earthquakes (REs) in the Ometepec–Pinotepa Nacional region (black square in Figure 1). (a) Number of REs detected in the region in 2-month bins (blue line). Red shaded areas show slow slip events (SSEs) in Guerrero, while blue areas show the time intervals of the SSEs in Oaxaca. (b) Cumulative number of REs in the Ometepec–Pinotepa Nacional region (blue line) and the Guerrero Gap (red). Blue stems denote earthquakes with magnitudes larger than $M_w \geq 6.0$, red stems, earthquakes with $M_w \geq 7.0$, and the green stem indicates the 2012 Ometepec earthquake. The yellow star marks the M_w 8.2 Tehuantepec earthquake.

relationship (black dashed line) after correcting for the local slip rate (i.e., the plate convergence rate) as shown in K. H. Chen et al. (2007). In contrast, the Ometepec–Pinotepa Nacional region (yellow-green colors) shows much shorter recurrence times likely due to the coseismic and postseismic perturbations induced by both the 2012 Ometepec and 2018 Pinotepa earthquakes. Another way to see this is shown in Figure 7, where the large differences in the recurrence times between the Ometepec–Pinotepa Nacional and adjacent segments are clear, dropping below the 1-month threshold in the former case. The recurrence time of these burst-type SSE conflict with the expected recurrence time even under the influence of aseismic slip. Events like this may occur off the main faults (Templeton et al., 2008) or may represent partial ruptures of a larger asperity (Canitano et al., 2021; Lengliné & Marsan, 2009). This situation only occurs for a handful of events when we impose a magnitude of completeness, $M_c \geq 3.8$. On the other hand, the postseismic relaxation produced by the 2014 Papanoa earthquake in Guerrero had a small effect on the recurrence times compared with nearby sequences, such as the GG, where recurrence times of most of the REs range between 1 and 10. A similar plot including all the stations available after 2012 including all detected events is shown in Figure S5 in Supporting Information S1.

To investigate possible changes in the slip rates along the adjacent areas of the rupture zones, we grouped the REs along four profiles as indicated in the map shown in Figure 4 (in each group, we include all epicenters within

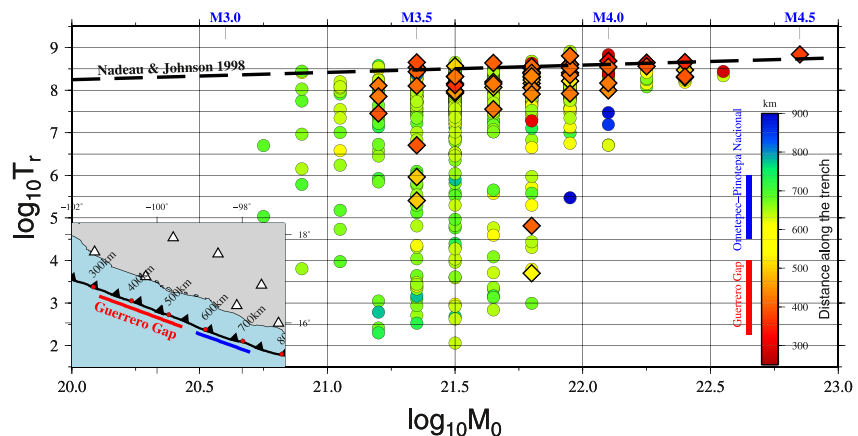


Figure 6. Comparison between the recurrence times along the Guerrero Gap and the Ometepec–Pinotepa Nacional region. Colors indicate the distance along the trench as indicated in the inset, diamond-type markers indicate the recurrence times of repeating earthquakes (REs) along the Guerrero Gap (GG), circles correspond to REs outside the GG mostly along the Ometepec–Pinotepa Nacional region. The dotted line indicates the expected recurrence times from the empirical relationship proposed by Nadeau and Johnson (1998).

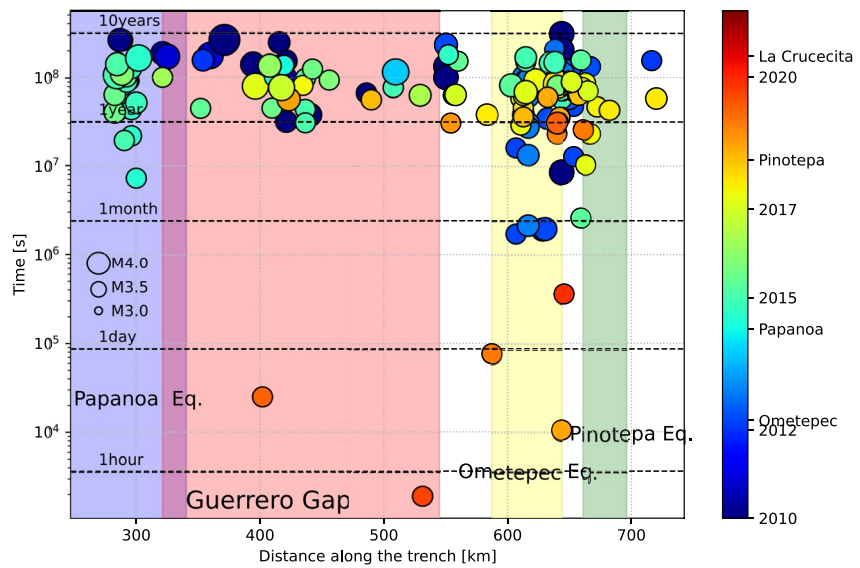


Figure 7. Recurrence times of reported repeating earthquake (RE) pairs color coded by the occurrence time of the first event in the sequence. The size of the circles is proportional to the average magnitude of the events. Shaded areas show the projected rupture areas of the 2014 Papanoa earthquake (blue), the Guerrero Gap (red), the 2012 Ometepec earthquake (yellow), and the 2018 Pinotepa earthquake (green). Only REs above the $M_c \geq 3.8$, excluding data from stations PEIG and YOIG are shown in this plot.

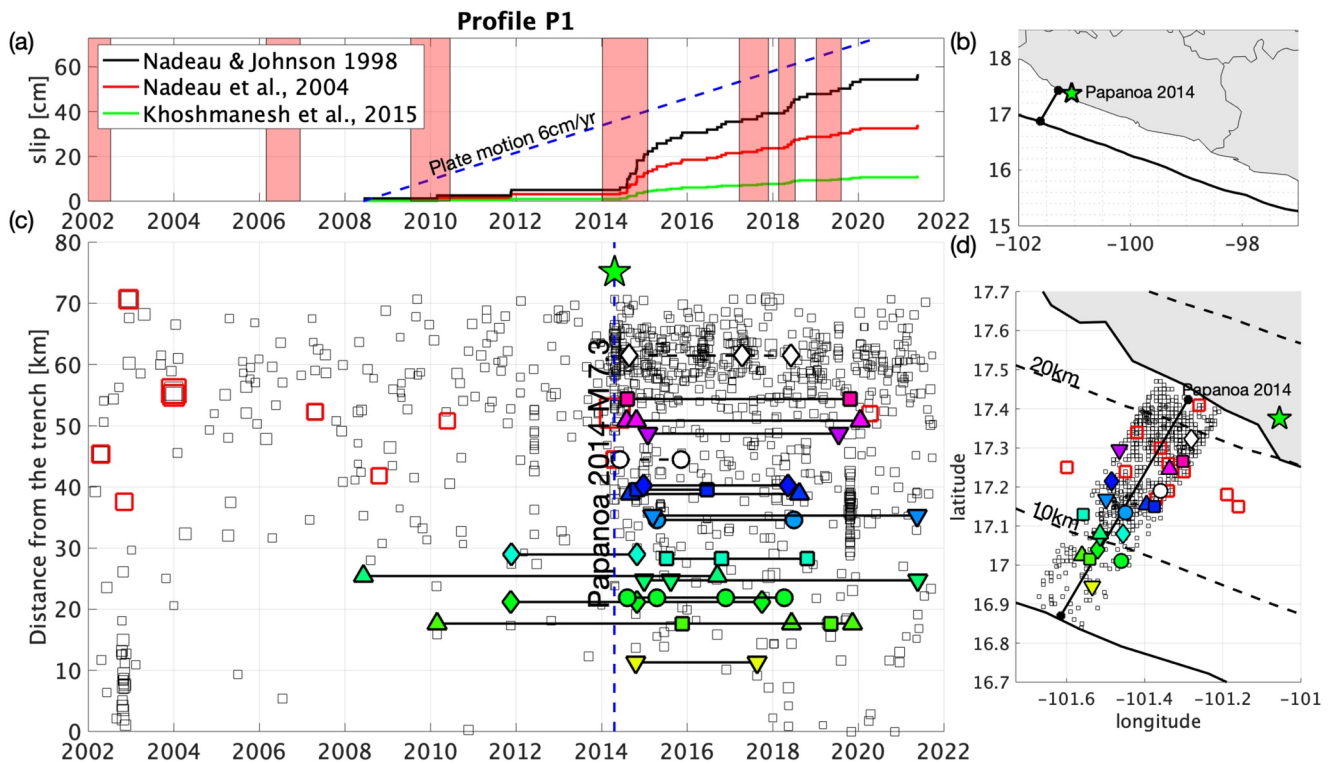


Figure 8. Seismicity and repeating earthquake (RE) activity along a profile P1, near the 2014 Papanoa earthquake (see Figure 4). (a) Estimated slip rates based on three empirical relationships (see main text), red shaded areas show the time windows for the slow slip event (SSE) in Guerrero. (b) Location map. (c) Temporal evolution of the seismicity before and after the 2014 Papanoa earthquake. Black squares indicate the reported seismicity along a 10 km strip at each profile side. Colored symbols indicate the occurrence of REs (white markers show REs below $M_c < 3.8$); red squares indicate $M \geq 5.0$. (d) Map view of the profile. Background seismicity is shown as empty squares; REs within in a 10 km distance from the profile, $M \geq 5.0$ within a 20 km distance from the profile are denoted by red open squares and the location of the 2014 Papanoa earthquake by the green star (a unique combination of color symbol is used in (c) and (d) to identify independent sequences).

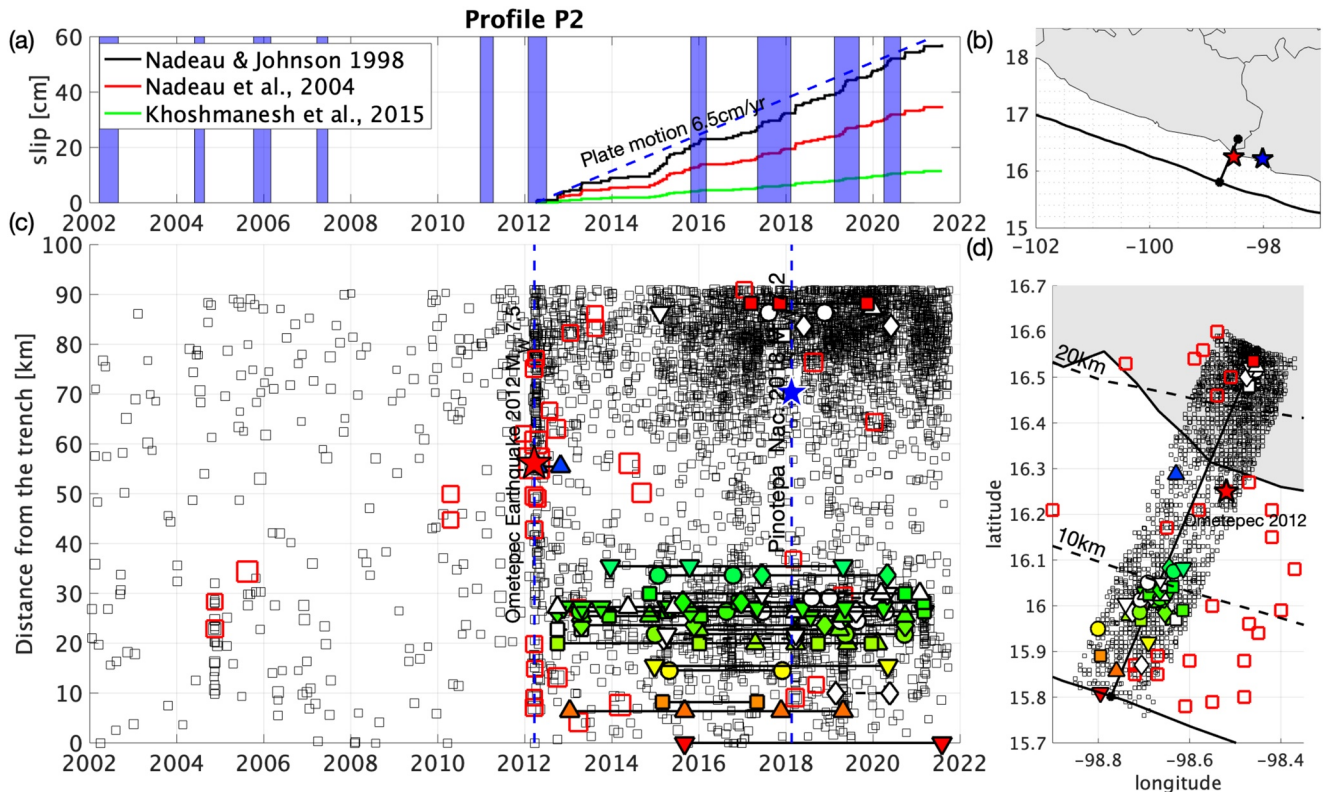


Figure 9. Seismicity and repeating earthquake (RE) activity along a profile P2 near the 2012 Ometepec and 2018 Pinotepa earthquakes (see Figure 4). (a) Estimated slip rates based on three empirical relationships (see main text), blue shaded areas show the time windows for the slow slip event (SSE) in Oaxaca. (b) Location map. (c) Temporal evolution of the seismicity, black squares indicate the reported seismicity along a 10 km strip at each side profile side. Colored symbols indicate the occurrence of REs (white markers show REs below the $M_c < 3.8$). (d) Map view of the profile. The seismicity is shown as empty black squares; REs as symbols color coded by distance to trench; the stars indicate the location of the 2012 Ometepec (blue) and 2018 Pinotepa (red) earthquakes (a unique combination of color symbol is used in (c) and (d) to identify independent sequences).

10 km of the lines). Profile P1 corresponds to a line perpendicular to the trench that aims toward the rupture area of the 2014 Papanoa earthquake west of the GG. Note that the 2014 Papanoa rupture took place during the 2014 Guerrero SSE, which likely acted as a triggering mechanism of the earthquake (Radiguet et al., 2016; UNAM Seismology Group, 2015). Figure 8 shows the evolution of the RE activity along this profile. RE detections start 6 years before the earthquake and updip, between 15 and 30 km from the trench, indicating possible slip acceleration in the shallow part of the plate interface. After the mainshock, new sequences developed downdip near the hypocenter, certainly associated with the postseismic relaxation for 2 years following the event. Southeast of the study region, profiles P2 and P3 (Figures 9 and 10, respectively) are parallel lines that extend approximately toward the rupture areas of the 2012 Ometepec and 2018 Pinotepa earthquakes. These profiles show a more intense aftershock activity that concentrates in the two different depth ranges, downdip around the 20 km depth interface and around the 10 km depth isoline (see Figure S6 in Supporting Information S1). The 2012 Ometepec and 2018 Pinotepa earthquakes nucleated at depths between 10 and 20 km, where the seismicity is significantly lower and where almost no repeaters are observed both before and after the events. This suggests the existence of either a relatively locked or freely slipping (stable) trench-parallel segment with 20–30 km in length along dip. Unlike profile P3, profile P2 shows a delayed activation of REs that happened in the shallow, near the trench segment (about 6 months after the 2012 Ometepec earthquake, between the 0 and 10 km isolines) and then in the deeper segment about 3 years later near the 20 km isoline. Although this deeper activity has magnitudes mostly below $M < 3.8$ (empty symbols, Figure 8d). In profile P3, RE activity began immediately after the mainshock in both segments with more intensity in the shallow one.

The most outstanding feature of the RE activity is the absence of repeaters for more than a decade before the 2012 earthquake, especially in the Ometepec region (Figures 9 and 10). After this event, seismicity (and REs) largely increased, as expected from the afterslip of the 2012 and 2018 earthquakes (UNAM Seismology

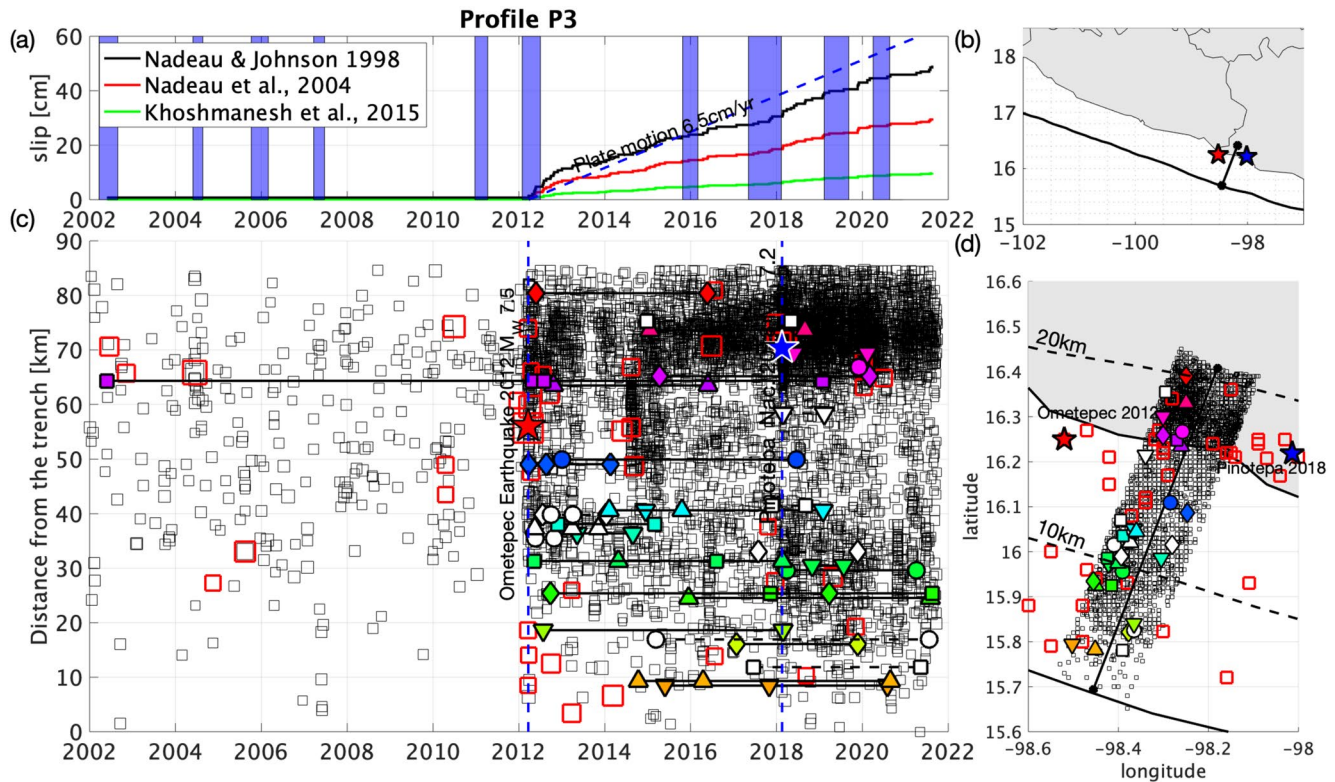


Figure 10. Seismicity and repeating earthquake (RE) activity along profile P3 near the 2018 Pinotepa earthquake (see Figure 4). (a) Estimated slip rates based on three empirical relationships (see main text), blue shaded areas show the time windows for the slow slip event (SSE) in Oaxaca. (b) Location map. (c) Temporal evolution of the seismicity before and after the 2018 Pinotepa earthquake. Black squares indicate the reported seismicity along a 10 km strip at each profile side. Colored symbols indicate the occurrence of RE (white markers show REs below the $M_c < 3.8$). (d) Map view of the profile; the seismicity is shown as empty squares; REs as symbols color coded by distance from the trench; the stars indicate the location of the 2012 Ometepec (blue) and the 2018 Pinotepa (red) earthquakes; red open squares show seismicity $M \geq 5.0$ within a 30 km distance from the profile (a unique combination of color symbol is used in (c) and (d) to identify independent sequences).

Group, 2013, 2015). The activation of REs (most of them offshore) from the occurrence of the 2012 event suggests two possibilities: (a) that the shallow plate-interface region mechanically transitioned from a predominantly locked to a weaker slipping regime when the earthquake happened; or (b) that the downdip segment unlocked after the event and pulled down (overstressed) the shallow block increasing the strain release rate updip. In both cases, the shallow offshore segment seems to have evolved from a quasi-static, creeping regime to an aseismic stress-releasing state (K. Wang & Dixon, 2004). Although the first hypothesis is plausible due to dynamic weakening of the fault gauge materials due to large seismic waves (Cruz-Atienza et al., 2021; Johnson et al., 2012), we favored the second hypothesis. The large afterslip produced by the Ometepec earthquake is most likely the main mechanism that activated RE in the updip portion. Similar behavior has been reported in Ecuador after the M_w 7.8 2016 Pedernales earthquake (Chalumeau et al., 2021) and in Taiwan after the M_L 6.3 2003 Chengkung earthquake (Y. Chen et al., 2020). In both cases, significantly larger slip rate and RE activation were reported after the main shock, but in the case of Mexico this may have a significant contribution in the nucleation of the 2018 Pinotepa earthquake. Furthermore, sustained seismic and RE activity continued until 2021, this could certainly be explained by the regional plate interface softening produced by seismic waves of the great M_w 8.2 (2017) Tehuantepec earthquake (Melgar, Pérez-Campos, et al., 2018; Meng et al., 2019; Suárez et al., 2019), which strongly disturbed the SSE cycles in Guerrero and Oaxaca (Cruz-Atienza et al., 2021).

Several empirical relationships have been proposed to estimate the fault slip at the interface based on the RE magnitude. Comparison between these relationships (Figures 8–10, panel a) shows very large differences that range from near plate convergence speed (Nadeau & Johnson, 1998) to near full coupled (Koshmanesh et al., 2015). Little can be said from this comparison. However, since the stress-releasing afterslip of both earthquakes spread partly across the RE locations, especially those below 10 km depth (Cruz-Atienza et al., 2021;

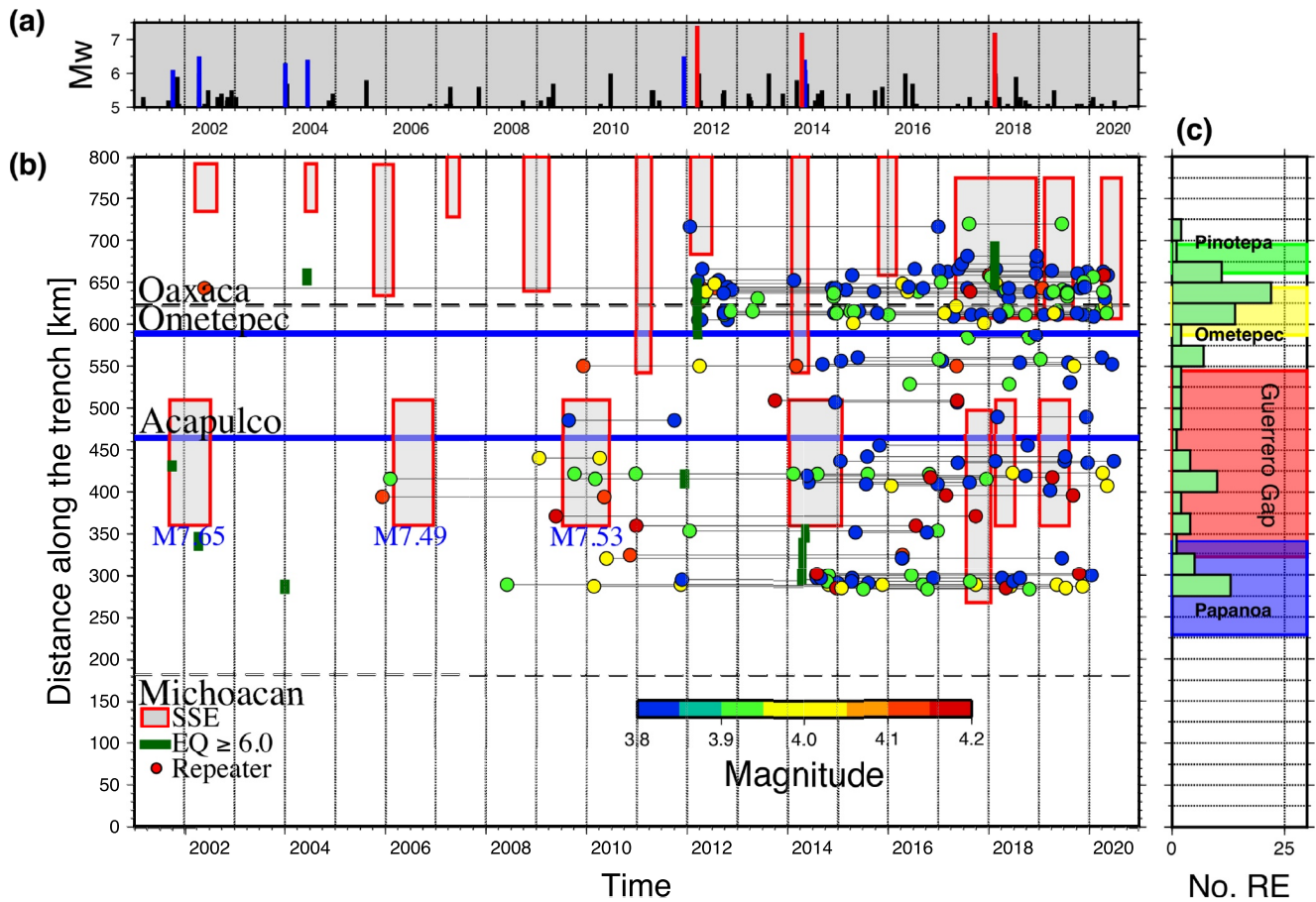


Figure 11. Temporal variations of the repeating earthquakes in Mexico above $M_c \geq 3.8$. (a) Timeline for events with magnitude $5.0 \leq M < 6.0$ (black bars), $6.0 \leq M < 7.0$ (blue bars), and $M \geq 7.0$ (red bars). (b) The y axis indicates the distance along the trench as indicated in Figure 4. Shaded areas show the approximate slow slip event (SSE) duration and along the trench projected areas. Blue lines indicate the projection to the distance along the trench of the cities of Acapulco and Ometepec. Repeating earthquakes (REs) are color coded by magnitude. Green bars indicate earthquake's occurrence and estimated length of earthquakes with a magnitude larger than 6.0. (c) Distribution of REs along the trench.

Graham et al., 2014), the relationship proposed by Koshmanesh et al. (2015) is clearly inappropriate for Oaxaca as it does not predict slip rates larger than the plate convergence velocity after the events. Precise parameter calibration in space and time requires further investigation to determine the best set of parameters (a and b , see Equation 1) that better describe the slip along the interface for the Mexican subduction zone. Figure S8 in Supporting Information S1 summarizes the possible slip for each profile using different empirical relationships and describes the slip variation along the trench.

Figure 11 shows the temporal distribution of the RE clusters projected along the trench as indicated in the map of Figure 4. Although we carefully determined the completeness cutoff magnitude for the whole region considering only available stations before 2012, the deficit of REs between 2001 and 2006 can be partially attributed to a sparser network and gaps in the data, as shown in Figures S1 and S2 in Supporting Information S1. However, the total absence of REs in the Oaxaca segment between 2006 and the 2012 Ometepec earthquake suggests a strong interface coupling in that period. By contrast, the opposite situation seems to dominate after this event, where large and sustained RE activity is found, that is, a large and sustained increase of the interplate slip rate. This conjecture is independently supported by the long-term GPS data in Pinotepa Nacional (i.e., PINO station collocated with the seismic station PNIG; Figure 12). Until the 2012 Ometepec earthquake, the station followed a steady-state northward motion as expected at this site by the regional plate convergence. However, after the rupture of the 2012 Ometepec earthquake, a large postseismic rebound was observed that lasted until 2016. During the 4 years of postseismic relaxation, the site steadily moved seawards (southward), indicating interplate slip rates larger than the plate convergence velocity. After the relaxation, the displacement partially recovered its

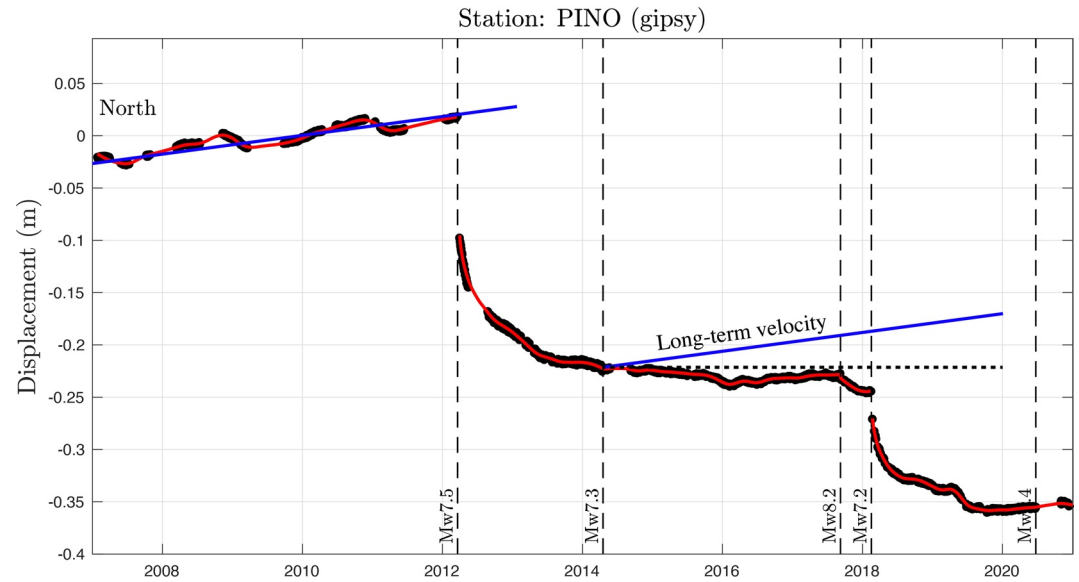


Figure 12. North displacement time series of the closest GPS station PINO (collocated with the seismic station PNIG). Black dots indicate corrected data, and the red solid line shows the interpolated signal. Dotted vertical lines indicate the time of the major earthquakes during this period (2007–2021). Blue lines show the expected long-term velocity rate before the occurrence of 2012 Ometepec earthquake. Horizontal dashed line indicates the no-displacement reference.

interseismic regime to the north until the great 2017 M_w 8.2 Tehuantepec earthquake perturbed the entire region, most likely leading the 2018 M_w 7.2 Pinotepa earthquake (Cruz-Atienza et al., 2021). In other words, during 2016 and until the Tehuantepec rupture on 8 September 2017, the upper plate at PNIG moved northward with speed smaller than the long-term expected velocity, which suggests a large creeping rate at the interface. These independent observations are consistent with the sustained increase of REs activity in the region between the Ometepec (2012) and Pinotepa (2018) earthquakes (Figures 9 and 10).

Conversely, along the GG, REs show a more steady behavior, probably affected by the occurrence of SSEs in Guerrero, as suggested in Figure 5. Before the 2006 SSE, repeaters preceded the onset of the event while during the 2009–2010 SSE, RE activity increased during this event as well as during the 2014 SSE. However, several REs may appear during the inter-SSE period of the 2014 and 2018 events. This correlation started to fade after 2017, most likely as a result of the seismic perturbation caused by the 8.2 Tehuantepec earthquake. The 2014 Papanoa earthquake gave rise to both activation of new RE clusters and reactivation of previously identified clusters mostly toward the west side of the rupture farther from the border of the GG, while inside the GG, a larger population of REs emerged after the 2014 SSE. A complementary and equivalent figure showing all the detected REs including those below our estimated time-independent magnitude of completeness (i.e., $M_c = 3.8$) is provided in Figure S7 in Supporting Information S1.

Figure 13 shows how RE activity evolved in Oaxaca during the interseismic period between the 2012 Ometepec and 2018 Pinotepa earthquakes. Circles indicate the location of the first event detected in each sequence color coded by decimal date. After the 2012 Ometepec earthquake, new REs appeared near the trench and along the border of the estimated rupture area of the 1968 earthquake (purple contour Figure 13b), toward the hypocenter of the 2018 Pinotepa earthquake. Furthermore, a significant number of new RE sequences reactivated close to the hypocenter starting in 2017 (blue markers Figure 13a) and new others appeared at the downdip edge of the second asperity proposed by Li et al. (2020) (yellow box in Figure 13b).

This intense RE activity strongly suggests the widespread aseismic slip occurring in the plate interface during the years following the 2012 Ometepec earthquake, which certainly reached shallow interface portions (i.e., above 10 km depth and probably next to the trench) and a large part of the 2018 earthquake rupture zone (both onshore and offshore, including the vicinity of the nucleation point) as previously noticed around the hypocentral region in an increase of foreshock seismicity (Cruz-Atienza et al., 2021).

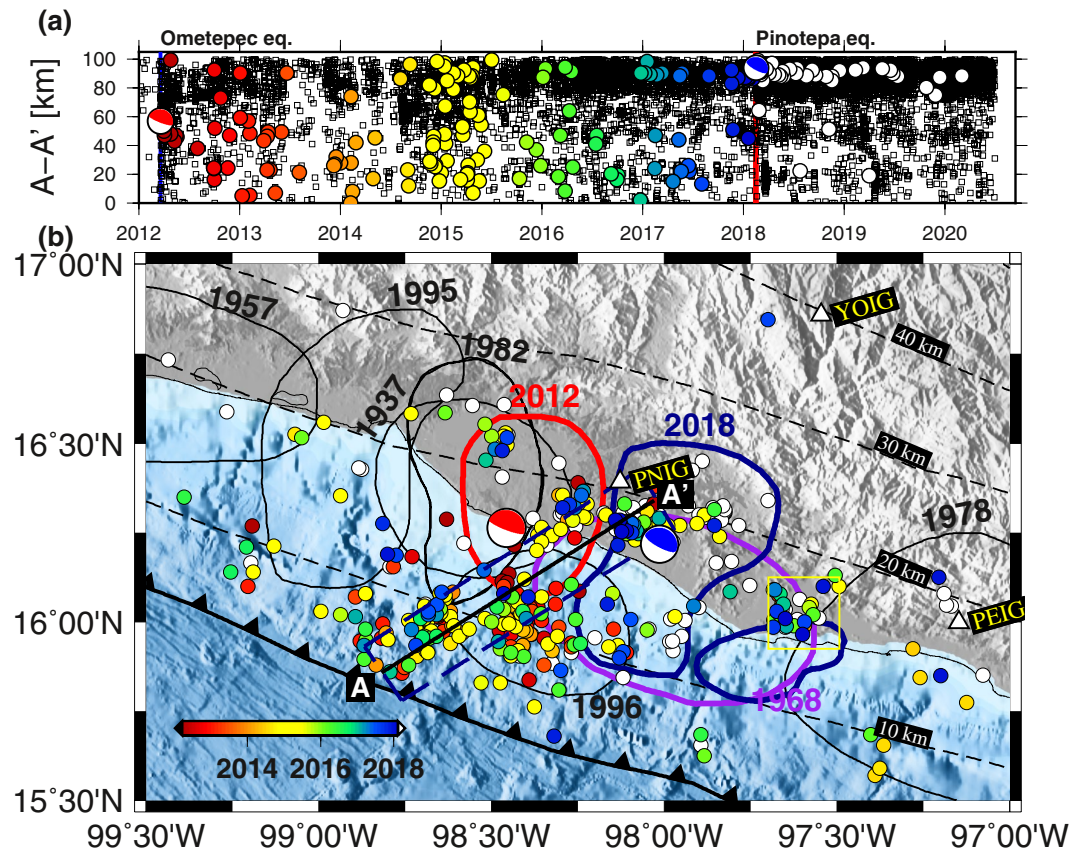


Figure 13. Repeating earthquake (RE) activation after the 2012 Ometepec earthquake. (a) Timeline showing the activation of REs along the A–A' profile, empty black squares show the background seismicity and colored circles indicate the first detected RE location within a sequence color coded by time of the first event in the sequence. White circles indicate those REs that appeared after the 2018 Pinotepa earthquake. (b) Map view. Blue contour and beach ball correspond to the rupture area of the 2012 Ometepec earthquake (UNAM Seismology Group, 2013); red contours and beach ball show the rupture area of the 2018 Pinotepa earthquake (Li et al., 2020); purple contour indicates the approximate rupture area of the 1968 earthquake. The yellow box shows a cluster of REs around the second asperity of the 2018 Pinotepa earthquake.

5. Conclusions

Our updated catalog of REs along the Mexican subduction zone provides a valuable tool to investigate how the interplate slip evolved during the last 20 years. This period is particularly interesting given the fact that for about 12 years (2001–2012) the subduction zone did not experience any large thrust earthquakes. During the following nine years (2012–2021), five $M7+$ class subduction events occurred in Guerrero and Oaxaca regions. We solved for both the stress drop and relative distance of the RE sequences to quantify the size of the asperities, their relative locations, overlap, and the associated interplate aseismic slip. Combining coda wave interferometry and solving the resulting distances using a genetic algorithm, we obtained a reliable catalog of REs above the completeness magnitude $M_c \geq 3.8$. From this analysis, the case of the Ometepec–Pinotepa Nacional segment in Oaxaca, where the 2012 earthquake gave rise to a long-lasting, sustained aseismic slip in the region that abruptly increased the RE activity, especially updip (above 15 km depth, mainly offshore), near the trench. During the years following this earthquake, REs activated in a broad region and concentrated next to both the updip edge of the 2018 Pinotepa rupture zone and its hypocenter further downdip. These observations strongly suggest that the shallow, offshore segment of the plate interface continuously slipped after the 2012 earthquake, which may have loaded a large part of the 2018 rupture area. Furthermore, in 2016, several new RE sequences appeared in between the rupture zones of both earthquakes, bordering what may have been the rupture area of the 1968 earthquake. All this activity along with the 2018 Oaxaca SSE that began in June 2017 and swept the downdip portion of the interface (Cruz-Atienza et al., 2021) was certainly responsible for the initiation and rupture propagation of

the Pinotepa earthquake. Furthermore, analysis along the GG shows a more dispersed distribution of RE with no significant temporal variations even after the 2014 Papanoa earthquake, whose RE sequences activated mostly sideways (West) of the epicentral area outside the GG. REs in this region are characterized by steady-state behavior with larger recurrence times (1–10 years), likely modulated by the occurrence of SSEs.

Data Availability Statement

The seismic data used for the detection of REs in this study are available at Zenodo via <https://doi.org/10.5281/zenodo.6471384>. Code for the inversion of the relative position of RE is available at <https://zenodo.org/record/6533824#.Ynl6fHVomdc>.

Acknowledgments

The Servicio Sismológico Nacional (Mexico) earthquake catalog is possible thanks to its personnel and product of the calculations made by its Analysis and Interpretation of Seismic Data department. SSN data were obtained by the Servicio Sismológico Nacional (México); station maintenance, data acquisition, and distribution are thanks to its personnel. GPS data for PINO station were processed by Sara Ivonne Franco at LaGeos laboratory, UNAM. This work was supported by UNAM-PAPIIT IN120220, IN116919, and IG100921, CONACyT grant 6471, NSF grant EAR-1735448, and SATREPS-UNAM grant 15543611. We made use of GMT, ZMAP, OBSPY, Tensorflow, and SAC software. We thank the associate editor, Satoshi Ide, and two anonymous reviewers for their helpful comments.

References

- Anderson, J., Quaa, R., Singh, S. K., Espinosa, J. M., Jimenez, A., Lermo, J., et al. (1995). The Copala, Guerrero, Mexico earthquake of September 14, 1995 ($M_w = 7.4$): A preliminary report. *Seismological Research Letters*, *66*(6), 11–39. <https://doi.org/10.1785/gssrl.66.6.11>
- Astiz, L., & Kanamori, H. (1984). An earthquake doublet in Ometepec, Guerrero, Mexico. *Physics of the Earth and Planetary Interiors*, *34*(1–2), 24–45. [https://doi.org/10.1016/0031-9201\(84\)90082-7](https://doi.org/10.1016/0031-9201(84)90082-7)
- Audet, P., & Kim, Y. (2016). Teleseismic constraints on the geological environment of deep episodic slow earthquakes in subduction zone forearcs: A review. *Tectonophysics*, *670*, 1–15. <https://doi.org/10.1016/j.tecto.2016.01.005>
- Audet, P., & Schwartz, S. (2013). Hydrologic control of forearc strength and seismicity in the Costa Rican subduction zone. *Nature Geosciences*, *6*, 852–855. <https://doi.org/10.1038/ngeo1927>
- Barbot, S., Lapusta, N., & Avouac, J. P. (2012). Under the hood of the earthquake machine: Toward predictive modeling of the seismic cycle. *Science*, *336*(6082), 707–710. <https://doi.org/10.1126/science.1218796>
- Boore, D. M., & Boatwright, J. (1984). Average body-wave radiation coefficients. *Bulletin of the Seismological Society of America*, *74*(5), 1615–1621. <https://doi.org/10.1785/bssa0740051615>
- Brune, J. N. (1970). Tectonic stress and the spectra of seismic shear waves from earthquakes. *Journal of Geophysical Research*, *75*(26), 4997–5009. <https://doi.org/10.1029/JB075i026p04997>
- Canitano, A., Godano, M., & Thomas, M. Y. (2021). Inherited state of stress as a key factor controlling slip and slip mode: Inference from the study of a slow slip event in the Longitudinal Valley, Taiwan. *Geophysical Research Letters*, *48*, e2020GL090278. <https://doi.org/10.1029/2020GL090278>
- Castellanos, J. C., Clayton, R. W., & Pérez-Campos, X. (2018). Imaging the eastern Trans-Mexican Volcanic Belt with ambient seismic noise: Evidence for a slab tear. *Journal of Geophysical Research: Solid Earth*, *123*, 7741–7759. <https://doi.org/10.1029/2018JB015783>
- Cattania, C., & Segall, P. (2019). Crack models of repeating earthquakes predict observed moment-recurrence scaling. *Journal of Geophysical Research: Solid Earth*, *124*, 476–503. <https://doi.org/10.1029/2018JB016056>
- Cesca, S., Malebrán, C. V., López-Comino, J. Á., Davis, T., Tassara, C., Oncken, O., & Dahm, T. (2021). The 2014 Juan Fernández microplate earthquake doublet: Evidence for large thrust faulting driven by microplate rotation. *Tectonophysics*, *801*, 228720. <https://doi.org/10.1016/j.tecto.2021.228720>
- Chalumeau, C., Agurto-Detzel, H., De Barros, L., Charvis, P., Galve, A., Rietbrock, A., et al. (2021). Repeating earthquakes at the edge of the afterslip of the 2016 Ecuadorian M_w 7.8 Pedernales earthquake. *Journal of Geophysical Research: Solid Earth*, *126*, e2021JB021746. <https://doi.org/10.1029/2021JB021746>
- Chaves, E. J., Schwartz, S. Y., & Abercrombie, R. E. (2020). Repeating earthquakes record fault weakening and healing in areas of megathrust postseismic slip. *Science Advances*, *6*(32), eaaz9317. <https://doi.org/10.1126/sciadv.aaz9317>
- Chen, K. H., Nadeau, R. M., & Rau, R. J. (2007). Towards a universal rule on the recurrence interval scaling of repeating earthquakes? *Geophysical Research Letters*, *34*, L16308. <https://doi.org/10.1029/2007GL030554>
- Chen, T., & Clayton, R. W. (2012). Structure of central and southern Mexico from velocity and attenuation tomography. *Journal of Geophysical Research*, *117*, B09302. <https://doi.org/10.1029/2012JB009233>
- Chen, T., & Lapusta, N. (2009). Scaling of small repeating earthquakes explained by interaction of seismic and aseismic slip in a rate and state fault model. *Journal of Geophysical Research*, *114*, B01311. <https://doi.org/10.1029/2008JB005749>
- Chen, Y., Chen, K. H., Hu, J.-C., & Lee, J.-C. (2020). Probing the variation in aseismic slip behavior around an active suture zone: Observations of repeating earthquakes in eastern Taiwan. *Journal of Geophysical Research: Solid Earth*, *124*, e2019JB018561. <https://doi.org/10.1029/2019JB018561>
- Cleveland, K. M., Ammon, C. J., & Lay, T. (2014). Large earthquake processes in the northern Vanuatu subduction zone. *Journal of Geophysical Research: Solid Earth*, *119*, 8866–8883. <https://doi.org/10.1002/2014JB011289>
- Corral, A. (2004). Long-term clustering, scaling, and universality in the temporal occurrence of earthquakes. *Physical Review Letters*, *92*(10), 108501. <https://doi.org/10.1103/physrevlett.92.108501>
- Cruz-Atienza, V. M., Husker, A., Legrand, D., Caballero, E., & Kostoglodov, V. (2015). Nonvolcanic tremor locations and mechanisms in Guerrero, Mexico, from energy-based and particle motion polarization analysis. *Journal of Geophysical Research: Solid Earth*, *120*, 275–289. <https://doi.org/10.1002/2014JB011389>
- Cruz-Atienza, V. M., Tago, J., Villafuerte, C., Wei, M., Garza-Girón, R., Dominguez, L. A., et al. (2021). Short-term interaction between silent and devastating earthquakes in Mexico. *Nature Communications*, *12*(1), 1–14. <https://doi.org/10.1038/s41467-021-22326-6>
- Cruz-Atienza, V. M., Villafuerte, C., & Bhat, H. S. (2018). Rapid tremor migration and pore-pressure waves in subduction zones. *Nature Communications*, *9*(1), 1–13. <https://doi.org/10.1038/s41467-018-05150-3>
- Dominguez, L. A., Taira, T. A., & Santoyo, M. A. (2016). Spatiotemporal variations of characteristic repeating earthquake sequences along the Middle America Trench in Mexico. *Journal of Geophysical Research: Solid Earth*, *121*, 8855–8870. <https://doi.org/10.1002/2016JB013242>
- Dziwonski, A. M., & Anderson, D. L. (1981). Preliminary reference Earth model. *Physics of the Earth and Planetary Interiors*, *25*(4), 297–356. [https://doi.org/10.1016/0031-9201\(81\)90046-7](https://doi.org/10.1016/0031-9201(81)90046-7)

- Eshelby, J. D. (1957). The determination of the elastic field of an ellipsoidal inclusion, and related problems. *Proceedings of the Royal Society of London. Series A. Mathematical and Physical Sciences*, 241(1226), 376–396.
- Fasola, S. L., Brudzinski, M. R., Holtkamp, S. G., Graham, S. E., & Cabral-Cano, E. (2019). Earthquake swarms and slow slip on a sliver fault in the Mexican subduction zone. *Proceedings of the National Academy of Sciences of the United States of America*, 116(15), 7198–7206. <https://doi.org/10.1073/pnas.1814205116>
- Ferrari, L., Orozco-Esquivel, T., Manea, V., & Manea, M. (2012). The dynamic history of the Trans-Mexican Volcanic Belt and the Mexico subduction zone. *Tectonophysics*, 522, 122–149. <https://doi.org/10.1016/j.tecto.2011.09.018>
- Gaite, B., Iglesias, A., Villaseñor, A., Herraiz, M., & Pacheco, J. F. (2012). Crustal structure of Mexico and surrounding regions from seismic ambient noise tomography. *Geophysical Journal International*, 188(3), 1413–1424. <https://doi.org/10.1111/j.1365-246x.2011.05339.x>
- García, D., Singh, S. K., Herraiz, M., Ordaz, M., Pacheco, J. F., & Cruz-Jiménez, H. (2009). Influence of subduction zone structure on coastal and inland attenuation in Mexico. *Geophysical Journal International*, 179(1), 215–230.
- García, D., Singh, S. K., Herraiz, M., Pacheco, J. F., & Ordaz, M. (2004). Inslab earthquakes of central Mexico: Q, source spectra, and stress drop. *Bulletin of the Seismological Society of America*, 94(3), 789–802.
- Graham, S. E., DeMets, C., Cabral-Cano, E., Kostoglodov, V., Walpersdorf, A., Cotte, N., et al. (2014). GPS constraints on the $M_w = 7.5$ Ometepec earthquake sequence, southern Mexico: Coseismic and post-seismic deformation. *Geophysical Journal International*, 199(1), 200–218. <https://doi.org/10.1093/gji/ggu167>
- Gualandi, A., Perfettini, H., Radiguet, M., Cotte, N., & Kostoglodov, V. (2017). GPS deformation related to the M_w 7.3, 2014, Papanoa earthquake (Mexico) reveals the aseismic behavior of the Guerrero seismic gap. *Geophysical Research Letters*, 44, 6039–6047. <https://doi.org/10.1002/2017GL072913>
- Horikawa, H. (2001). Earthquake doublet in Kagoshima, Japan: Rupture of asperities in a stress shadow. *Bulletin of the Seismological Society of America*, 91(1), 112–127. <https://doi.org/10.1785/0119990131>
- Hughes, L., Chamberlain, C. J., Townend, J., & Thomas, A. M. (2021). A repeating earthquake catalog from 2003 to 2020 for the Raukumara Peninsula, northern Hikurangi subduction margin, New Zealand. *Geochemistry, Geophysics, Geosystems*, 22, e2021GC009670. <https://doi.org/10.1029/2021GC009670>
- Husker, A., & Davis, P. M. (2009). Tomography and thermal state of the Cocos plate subduction beneath Mexico City. *Journal of Geophysical Research*, 114, B04306. <https://doi.org/10.1029/2008JB006039>
- Husker, A., Ferrari, L., Arango-Galván, C., Corbo-Camargo, F., & Arzate-Flores, J. A. (2018). A geologic recipe for transient slip within the seismogenic zone: Insight from the Guerrero seismic gap, Mexico. *Geology*, 46(1), 35–38. <https://doi.org/10.1130/g39202.1>
- Husker, A., Frank, W. B., Gonzalez, G., Avila, L., Kostoglodov, V., & Kazachkina, E. (2019). Characteristic tectonic tremor activity observed over multiple slow slip cycles in the Mexican subduction zone. *Journal of Geophysical Research: Solid Earth*, 124, 599–608. <https://doi.org/10.1029/2018JB016517>
- Husker, A. L., Kostoglodov, V., Cruz-Atienza, V. M., Legrand, D., Shapiro, N. M., Payero, J. S., et al. (2012). Temporal variations of non-volcanic tremor (NVT) locations in the Mexican subduction zone: Finding the NVT sweet spot. *Geochemistry, Geophysics, Geosystems*, 13, Q03011. <https://doi.org/10.1029/2011GC003916>
- Iglesias, A., Clayton, R. W., Pérez-Campos, X., Singh, S. K., Pacheco, J. F., Garcia, D., & Valdes-Gonzalez, C. (2010). S wave velocity structure below central Mexico using high-resolution surface wave tomography. *Journal of Geophysical Research*, 115, B06307. <https://doi.org/10.1029/2009JB006332>
- Johnson, P. A., Carpenter, B., Knuth, M., Kaproth, B. M., Le Bas, P.-Y., Daub, E. G., & Marone, C. (2012). Nonlinear dynamical triggering of slow slip on simulated earthquake faults with implications to Earth. *Journal of Geophysical Research*, 117, B04310. <https://doi.org/10.1029/2011JB008594>
- Kagan, Y. Y. (2011). Random stress and Omori's law. *Geophysical Journal International*, 186(3), 1347–1364. <https://doi.org/10.1111/j.1365-246x.2011.05114.x>
- Kagan, Y. Y., & Jackson, D. D. (1991). Long-term earthquake clustering. *Geophysical Journal International*, 104(1), 117–134. <https://doi.org/10.1111/j.1365-246x.1991.tb02498.x>
- Kagan, Y. Y., & Jackson, D. D. (1999). Worldwide doublets of large shallow earthquakes. *Bulletin of the Seismological Society of America*, 89(5), 1147–1155. <https://doi.org/10.1785/bssa0890051147>
- Kanamori, H. (1981). The nature of seismicity patterns before large earthquakes. In D. W. Simpson & P. G. Richards (Eds.), *Earthquake prediction. Maurice Ewing Series* (pp. 1–19). American Geophysical Union.
- Kazachkina, E., Kostoglodov, V., Cotte, N., Walpersdorf, A., Ramirez-Herrera, M. T., Gaidzik, K., et al. (2020). Active 650-km long fault system and Xolapa sliver in southern Mexico. *Frontiers of Earth Science*, 8, 155. <https://doi.org/10.3389/feart.2020.00155>
- Kazachkina, E., Kostoglodov, V., Husker, A., & Cotte, N. (2019). Activity of crustal faults and the Xolapa sliver motion in Guerrero–Oaxaca forearc of Mexico, from seismic data. *Earth, Planets and Space*, 71(1), 104. <https://doi.org/10.1186/s40623-019-1084-9>
- Keilis-Borok, V. I., Knopoff, L., & Rotvain, I. M. (1980). Bursts of aftershocks, long-term precursors of strong earthquakes. *Nature*, 283(5744), 259–263. <https://doi.org/10.1038/283259a0>
- Khoshmanesh, M., Shirzaei, M., & Nadeau, R. M. (2015). Time-dependent model of aseismic slip on the central San Andreas Fault from InSAR time series and repeating earthquakes. *Journal of Geophysical Research: Solid Earth*, 120, 6658–6679. <https://doi.org/10.1002/2015JB012039>
- Kim, Y., Clayton, R. W., Asimow, P. D., & Jackson, J. M. (2013). Generation of talc in the mantle wedge and its role in subduction dynamics in central Mexico. *Earth and Planetary Science Letters*, 384, 81–87. <https://doi.org/10.1016/j.epsl.2013.10.006>
- Konca, A. O., Avouac, J. P., Sladen, A., Meltzner, A. J., Sieh, K., Fang, P., et al. (2008). Partial rupture of a locked patch of the Sumatra megathrust during the 2007 earthquake sequence. *Nature*, 456(7222), 631–635. <https://doi.org/10.1038/nature07572>
- Kostoglodov, V., Husker, A., Shapiro, N. M., Payero, J. S., Campillo, M., Cotte, N., & Clayton, R. (2010). The 2006 slow slip event and nonvolcanic tremor in the Mexican subduction zone. *Geophysical Research Letters*, 37, L24301. <https://doi.org/10.1029/2010GL045424>
- Kostoglodov, V., & Pacheco, J. (1999). *Cien Años de Sismicidad en México*. Instituto de Geofísica, UNAM. <http://usuarios.geofisica.unam.mx/vladimir/sismos/100a%F1os.html>
- Lay, T., Ammon, C. J., Kanamori, H., Rivera, L., Koper, K. D., & Hutko, A. R. (2010). The 2009 Samoa–Tonga great earthquake triggered doublet. *Nature*, 466(7309), 964–968. <https://doi.org/10.1038/nature09214>
- Lay, T., Kanamori, H., Ammon, C. J., Hutko, A. R., Furlong, K., & Rivera, L. (2009). The 2006–2007 Kuril Islands great earthquake sequence. *Journal of Geophysical Research*, 114, B11308. <https://doi.org/10.1029/2008JB006280>
- Legrand, D., Iglesias, A., Singh, S. K., Cruz-Atienza, V., Yoon, C., Dominguez, L. A., et al. (2021). The influence of fluids in the unusually high-rate seismicity in the Ometepec segment of the Mexican subduction zone. *Geophysical Journal International*, 226(1), 524–535. <https://doi.org/10.1093/gji/ggab106>

- Lengliné, O., & Marsan, D. (2009). Inferring the coseismic and postseismic stress changes caused by the 2004 $M_w = 6$ Parkfield earthquake from variations of recurrence times of microearthquakes. *Journal of Geophysical Research*, *114*, B10303. <https://doi.org/10.1029/2008JB006118>
- Li, Y., Shan, X., Zhu, C., Qiao, X., Zhao, L., & Qu, C. (2020). Geodetic model of the 2018 M_w 7.2 Pinotepa, Mexico, earthquake inferred from InSAR and GPS data. *Bulletin of the Seismological Society of America*, *110*(3), 1115–1124. <https://doi.org/10.1785/0120190101>
- Lonsdale, P. (2005). Creation of the Cocos and Nazca plates by fission of the Farallon plate. *Tectonophysics*, *404*(3–4), 237–264. <https://doi.org/10.1016/j.tecto.2005.05.011>
- Madariaga, R. (1976). Dynamics of an expanding circular fault. *Bulletin of the Seismological Society of America*, *66*(3), 639–666. <https://doi.org/10.1785/bssa0660030639>
- Materna, K., Taira, T., & Bürgmann, R. (2018). Aseismic transform fault slip at the Mendocino Triple Junction from characteristically repeating earthquakes. *Geophysical Research Letters*, *45*, 699–707. <https://doi.org/10.1002/2017GL075899>
- Maury, J., Ide, S., Cruz-Atienza, V. M., & Kostoglodov, V. (2018). Spatiotemporal variations in slow earthquakes along the Mexican subduction zone. *Journal of Geophysical Research: Solid Earth*, *123*, 1559–1575. <https://doi.org/10.1002/2017JB014690>
- Maury, J., Ide, S., Cruz-Atienza, V. M., Kostoglodov, V., González-Molina, G., & Pérez-Campos, X. (2016). Comparative study of tectonic tremor locations: Characterization of slow earthquakes in Guerrero, Mexico. *Journal of Geophysical Research: Solid Earth*, *121*, 5136–5151. <https://doi.org/10.1002/2016JB013027>
- Mavrommatis, A. P., Segall, P., Uchida, N., & Johnson, K. M. (2015). Long-term acceleration of aseismic slip preceding the M_w 9 Tohoku-oki earthquake: Constraints from repeating earthquakes. *Geophysical Research Letters*, *42*, 9717–9725. <https://doi.org/10.1002/2015GL066069>
- Melgar, D., & Pérez-Campos, X. (2011). Imaging the Moho and subducted oceanic crust at the Isthmus of Tehuantepec, Mexico, from receiver functions. *Pure and Applied Geophysics*, *168*(8), 1449–1460. <https://doi.org/10.1007/s00024-010-0199-5>
- Melgar, D., Pérez-Campos, X., Ramirez-Guzman, L., Spica, Z., Espíndola, V. H., Hammond, W. C., & Cabral-Cano, E. (2018). Bend faulting at the edge of a flat slab: The 2017 M_w 7.1 Puebla–Morelos, Mexico earthquake. *Geophysical Research Letters*, *45*, 2633–2641. <https://doi.org/10.1002/2017GL076895>
- Melgar, D., Ruiz-Angulo, A., Garcia, E. S., Manea, M., Manea, V. C., Xu, X., et al. (2018). Deep embrittlement and complete rupture of the lithosphere during the M_w 8.2 Tehuantepec earthquake. *Nature Geoscience*, *11*(12), 955–960. <https://doi.org/10.1038/s41561-018-0229-y>
- Meng, L., Huang, H., Xie, Y., Bao, H., & Dominguez, L. A. (2019). Nucleation and kinematic rupture of the 2017 M_w 8.2 Tehuantepec earthquake. *Geophysical Research Letters*, *46*, 3745–3754. <https://doi.org/10.1029/2018GL081074>
- Moreno, M., Haberland, C., Oncken, O., Rietbrock, A., Angiboust, S., & Heidbach, O. (2014). Locking of the Chile subduction zone controlled by fluid pressure before the 2010 earthquake. *Nature Geoscience*, *7*(4), 292–296. <https://doi.org/10.1038/ngeo2102>
- Nadeau, R. M., & Johnson, L. R. (1998). Seismological studies at Parkfield VI: Moment release rates and estimates of source parameters for small repeating earthquakes. *Bulletin of the Seismological Society of America*, *88*(3), 790–814.
- Nadeau, R. M., & McEvilly, T. V. (1999). Fault slip rates at depth from recurrence intervals of repeating microearthquakes. *Science*, *285*(5428), 718–721. <https://doi.org/10.1126/science.285.5428.718>
- Nadeau, R. M., & McEvilly, T. V. (2004). Periodic pulsing of characteristic microearthquakes on the San Andreas fault. *Science*, *303*(5655), 220–222. <https://doi.org/10.1126/science.1090353>
- Nishenko, S. P., & Singh, S. K. (1987). The Acapulco–Ometepec, Mexico, earthquakes of 1907–1982: Evidence for a variable recurrence history. *Bulletin of the Seismological Society of America*, *77*(4), 1359–1367.
- Ordaz, M., & Singh, S. K. (1992). Source spectra and spectral attenuation of seismic waves from Mexican earthquakes, and evidence of amplification in the hill zone of Mexico City. *Bulletin of the Seismological Society of America*, *82*(1), 24–43.
- Ortiz, M., Singh, S. K., Kostoglodov, V., & Pacheco, J. (2000). Source areas of the Acapulco–San Marcos, Mexico earthquakes of 1962 (M 7.1; 7.0) and 1957 (M 7.7), as constrained by tsunami and uplift records. *Geofísica Internacional*, *39*(4), 337–348. <https://doi.org/10.22201/igeof.00167169p.2000.39.4.244>
- Pardo, M., & Suárez, G. (1995). Shape of the subducted Rivera and Cocos plates in southern Mexico: Seismic and tectonic implications. *Journal of Geophysical Research*, *100*(B7), 12357–12373. <https://doi.org/10.1029/95JB00919>
- Payero, J. S., Kostoglodov, V., Shapiro, N., Mikumo, T., Iglesias, A., Pérez-Campos, X., & Clayton, R. W. (2008). Nonvolcanic tremor observed in the Mexican subduction zone. *Geophysical Research Letters*, *35*, L07305. <https://doi.org/10.1029/2007GL032877>
- Pérez-Campos, X., Espíndola, V. H., Pérez, J., Estrada, J. A., Monroy, C. C., & Bello, D. (2018). The Mexican National Seismological Service: An Overview. *Seismological Research Letters*, *89*, 318–323. <https://doi.org/10.1785/0220170186>
- Pérez-Campos, X., Espíndola, V. H., Pérez, J., Estrada, J. A., Monroy, C. C., Fabila, B. Z., et al. (2019). Servicio Sismológico Nacional, Mexico. *Summary of the Bulletin of the International Seismological Centre*, *53*(II), 29–40. <https://doi.org/10.31905/SZ7RYBTM>
- Pérez-Campos, X., Kim, Y., Husker, A., Davis, P. M., Clayton, R. W., Iglesias, A., et al. (2008). Horizontal subduction and truncation of the Cocos Plate beneath central Mexico. *Geophysical Research Letters*, *35*, L18303. <https://doi.org/10.1029/2008GL035127>
- Plata-Martínez, R., Ide, S., Shinohara, M., Garcia, E. S., Mizuno, N., Dominguez, L. A., et al. (2021). Shallow slow earthquakes to decipher future catastrophic earthquakes in the Guerrero seismic gap. *Nature Communications*, *12*(1), 1–8. <https://doi.org/10.1038/s41467-021-24210-9>
- Plata-Martínez, R., Pérez-Campos, X., & Singh, S. K. (2019). Spatial distribution of radiated seismic energy of three aftershocks sequences at Guerrero, Mexico, subduction zone. *Bulletin of the Seismological Society of America*, *109*(6), 2556–2566. <https://doi.org/10.1785/0120190104>
- Poupinet, G., Ellsworth, W. L., & Frechet, J. (1984). Monitoring velocity variations in the crust using earthquake doublets: An application to the Calaveras Fault, California. *Journal of Geophysical Research*, *89*(B7), 5719–5731. <https://doi.org/10.1029/JB089iB07p05719>
- Prieto, G. A. (2022). The multitaper spectrum analysis package in Python. *Seismological Research Letters*, *93*(3), 1922–1929. <https://doi.org/10.1785/0220210332>
- Radiguet, M., Cotton, F., Vergnolle, M., Campillo, M., Walpersdorf, A., Cotte, N., & Kostoglodov, V. (2012). Slow slip events and strain accumulation in the Guerrero Gap, Mexico. *Journal of Geophysical Research*, *117*, B04305. <https://doi.org/10.1029/2011JB008801>
- Radiguet, M., Perfettini, H., Cotte, N., Gualandri, A., Valette, B., Kostoglodov, V., et al. (2016). Triggering of the 2014 M_w 7.3 Papanoa earthquake by a slow slip event in Guerrero, Mexico. *Nature Geoscience*, *9*(11), 829–833. <https://doi.org/10.1038/ngeo2817>
- Ramírez-Herrera, M. T., Gaidzik, K., Forman, S., Kostoglodov, V., Bürgmann, R., & Johnson, C. W. (2018). Relating the long-term and short-term vertical deformation across a transect of the forearc in the central Mexican subduction zone (2018). *Geosphere*, *14*(2), 419–439. <https://doi.org/10.1130/GES01446.1>
- Rivet, D., Campillo, M., Radiguet, M., Zigone, D., Cruz-Atienza, V., Shapiro, N. M., et al. (2014). Seismic velocity changes, strain rate and non-volcanic tremors during the 2009–2010 slow slip event in Guerrero, Mexico. *Geophysical Journal International*, *196*(1), 447–460. <https://doi.org/10.1093/gji/ggt374>
- Santoyo, M. A., Singh, S. K., Mikumo, T., & Ordaz, M. (2005). Space–time clustering of large thrust earthquakes along the Mexican subduction zone: An evidence of source stress interaction. *Bulletin of the Seismological Society of America*, *95*(5), 1856–1864. <https://doi.org/10.1785/0120040185>

- Sawires, R., Santoyo, M. A., Peláez, J. A., & Fernández, R. D. C. (2019). An updated and unified earthquake catalog from 1787 to 2018 for seismic hazard assessment studies in Mexico. *Scientific Data*, 6(1), 1–14. <https://doi.org/10.1038/s41597-019-0234-z>
- Segou, M., & Parsons, T. (2018). Testing earthquake links in Mexico from 1978 to the 2017 $M = 8.1$ Chiapas and $M = 7.1$ Puebla shocks. *Geophysical Research Letters*, 45, 708–714. <https://doi.org/10.1002/2017GL076237>
- Servicio Sismológico Nacional (SSN). (2021). Catálogo de sismos. Retrieved from <http://www2.ssn.unam.mx:8080/catalogo/>
- Shearer, P. M. (2019). *Introduction to seismology*. Cambridge University Press.
- Singh, S. K., Astiz, L., & Havskov, J. (1981). Seismic gaps and recurrence periods of large earthquakes along the Mexican subduction zone: A reexamination. *Bulletin of the Seismological Society of America*, 71(3), 827–843. <https://doi.org/10.1785/bssa0710030827>
- Singh, S. K., Pacheco, J., Courboux, F., & Novelo, D. A. (1997). Source parameters of the Pinotepa Nacional, Mexico, earthquake of 27 March, 1996 ($M_w = 5.4$) estimated from near-field recordings of a single station. *Journal of Seismology*, 1(1), 39–45. <https://doi.org/10.1023/a:1009741712512>
- Singh, S. K., Reinoso, E., Arroyo, D., Ordaz, M., Cruz-Atienza, V., Pérez-Campos, X., et al. (2018). Deadly intraslab Mexico earthquake of 19 September 2017 ($M_w 7.1$): Ground motion and damage pattern in Mexico City. *Seismological Research Letters*, 89(6), 2193–2203. <https://doi.org/10.1785/0220180159>
- Skinner, S. M., & Clayton, R. W. (2011). An evaluation of proposed mechanisms of slab flattening in central Mexico. *Pure and Applied Geophysics*, 168(8–9), 1461–1474. <https://doi.org/10.1007/s00024-010-0200-3>
- Sniieder, R., & Vrijlandt, M. (2005). Constraining the source separation with coda wave interferometry: Theory and application to earthquake doublets in the Hayward fault, California. *Journal of Geophysical Research*, 110, B04301. <https://doi.org/10.1029/2004JB003317>
- Spica, Z., Pertou, M., Calò, M., Legrand, D., Córdoba-Montiel, F., & Iglesias, A. (2016). 3-D shear wave velocity model of Mexico and south US: Bridging seismic networks with ambient noise cross-correlations (C1) and correlation of coda of correlations (C3). *Geophysical Journal International*, 206(3), 1795–1813. <https://doi.org/10.1093/gji/ggw240>
- Stein, S., & Liu, M. (2009). Long aftershock sequences within continents and implications for earthquake hazard assessment. *Nature*, 462(7269), 87–89. <https://doi.org/10.1038/nature08502>
- Storn, R., & Price, K. (1997). Differential evolution—A simple and efficient heuristic for global optimization over continuous spaces. *Journal of Global Optimization*, 11(4), 341–359. <https://doi.org/10.1023/A:1008202821328>
- Stubailo, I., Beghein, C., & Davis, P. M. (2012). Structure and anisotropy of the Mexico subduction zone based on Rayleigh-wave analysis and implications for the geometry of the Trans-Mexican Volcanic Belt. *Journal of Geophysical Research*, 117, B05303. <https://doi.org/10.1029/2011JB008631>
- Suárez, G., Santoyo, M. A., Hjørleifsdóttir, V., Iglesias, A., Villafuerte, C., & Cruz-Atienza, V. M. (2019). Large scale lithospheric detachment of the downgoing Cocos plate: The 8 September 2017 earthquake ($M_w 8.2$). *Earth and Planetary Science Letters*, 509, 9–14. <https://doi.org/10.1016/j.epsl.2018.12.018>
- Templeton, D. C., Nadeau, R. M., & Bürgmann, R. (2008). Behavior of repeating earthquake sequences in central California and the implications for subsurface fault creep. *Bulletin of the Seismological Society of America*, 98(1), 52–65. <https://doi.org/10.1785/0120070026>
- Tepp, G. (2018). A repeating event sequence alarm for monitoring volcanoes. *Seismological Research Letters*, 89(5), 1863–1876. <https://doi.org/10.1785/0220170263>
- Uchida, N. (2019). Detection of repeating earthquakes and their application in characterizing slow fault slip. *Progress in Earth and Planetary Science*, 6(1), 1–21. <https://doi.org/10.1186/s40645-019-0284-z>
- Uchida, N., Kalafat, D., Pinar, A., & Yamamoto, Y. (2019). Repeating earthquakes and interplate coupling along the western part of the North Anatolian Fault. *Tectonophysics*, 769, 228185. <https://doi.org/10.1016/j.tecto.2019.228185>
- Uchida, N., Shimamura, K., Matsuzawa, T., & Okada, T. (2015). Postseismic response of repeating earthquakes around the 2011 Tohoku-oki earthquake: Moment increases due to the fast loading rate. *Journal of Geophysical Research: Solid Earth*, 120, 259–274. <https://doi.org/10.1002/2013JB010933>
- Universidad Nacional Autónoma de México (UNAM) Seismology Group. (2013). Ometepec–Pinotepa Nacional, Mexico earthquake of 20 March 2012 ($M_w 7.5$): A preliminary report. *Geofísica Internacional*, 52, 172–196. [https://doi.org/10.1016/S0016-7169\(13\)71471-5](https://doi.org/10.1016/S0016-7169(13)71471-5)
- Universidad Nacional Autónoma de México (UNAM) Seismology Group. (2015). Papanoa, Mexico earthquake of 18 April 2014 ($M_w 7.3$). *Geofísica Internacional*, 54, 363–386. http://www.scielo.org.mx/scielo.php?pid=S0016-71692015000400363&script=sci_abstract&tlng=pt
- Vergnolle, M., Walpersdorf, A., Kostoglodov, V., Tregoning, P., Santiago, J. A., Cotte, N., & Franco, S. I. (2010). Slow slip events in Mexico revised from the processing of 11 year GPS observations. *Journal of Geophysical Research*, 115, B08403. <https://doi.org/10.1029/2009JB006852>
- Vidale, J. E., Ellsworth, W. L., Cole, A., & Marone, C. (1994). Variations in the rupture process with recurrence interval in a repeated small earthquake. *Nature*, 368(6472), 624–626. <https://doi.org/10.1038/368624a0>
- Villafuerte, C., & Cruz-Atienza, V. M. (2017). Insights into the causal relationship between slow slip and tectonic tremor in Guerrero, Mexico. *Journal of Geophysical Research: Solid Earth*, 122, 6642–6656. <https://doi.org/10.1002/2017JB014037>
- Wang, K., & Dixon, T. (2004). “Coupling” semantics and science in earthquake research. *Eos, Transactions, American Geophysical Union*, 85(18), 180. <https://doi.org/10.1029/2004EO180005>
- Wang, Q., Jackson, D. D., & Zhuang, J. (2010). Missing links in earthquake clustering models. *Geophysical Research Letters*, 37, L21307. <https://doi.org/10.1029/2010GL044858>
- Warren-Smith, E., Fry, B., Wallace, L., Chon, E., Henrys, S., Sheehan, A., et al. (2019). Episodic stress and fluid pressure cycling in subducting oceanic crust during slow slip. *Nature Geoscience*, 12(6), 475–481. <https://doi.org/10.1038/s41561-019-0367-x>
- Wyss, M., & Habermann, R. E. (1988). Precursory seismic quiescence. *Pure and Applied Geophysics*, 126(2–4), 319–332. <https://doi.org/10.1007/bf00879001>
- Yamamoto, J., Quintanar, L., & Jiménez, Z. (2002). Why earthquake doublets in the Ometepec, Guerrero, Mexico subduction area? *Physics of the Earth and Planetary Interiors*, 132(1–3), 131–139. [https://doi.org/10.1016/s0031-9201\(02\)00048-1](https://doi.org/10.1016/s0031-9201(02)00048-1)
- Yin-Tung, Y., Kuo-Fong, M., & Yi-Ying, W. (2008). Slip partition of the 26 December 2006 Pingtung, Taiwan ($M 6.9$, $M 6.8$) earthquake doublet determined from teleseismic waveforms. *TAO: Terrestrial, Atmospheric and Oceanic Sciences*, 19(6), 5.